AFML-TR-69-202

THE EFFECT OF PROJECTILE SHAPE ON THE BALLISTIC PERFORATION OF THIN METAL PLATES

MAJ. THOMAS E. FIELDS

TECHNICAL REPORT AFML-TR-69-202

JULY 1969

AIR FORCE MATERIALS LABORATORY
AIR FORCE SYSTEMS COMMAND
WRIGHT-PATTERSON AIR FORCE BASE, OHIO

NOTICES

When Government drawings, specifications, or other data are used for any purpose other than in connection with a definitely related Government procurement operation, the United States Government thereby incurs no responsibility nor any obligation whatsoever; and the fact that the Government may have formulated, furnisher, or in any way supplied the said drawings, specifications, or other data, is not to be regarded by implication or otherwise as in any manner licensing the holder or any other person or corporation, or conveying any rights or permission to manufacture, use, or sell any patented invention that may in any way be related thereto.

This document has been approved for public release and sale; its distribution is unlimited.

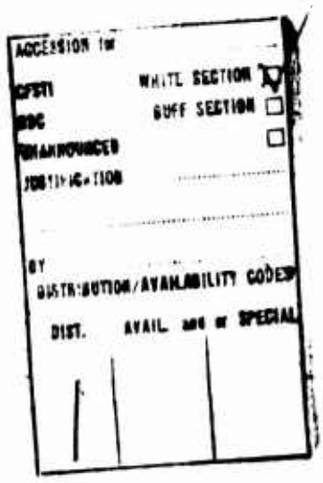

Copies of this report should not be returned unless return is required by security considerations, contractual obligations, or notice on a specific document.

300 - September 1969 - CO455 - 89-1974

BLANK PAGE

AFML-TR-69-202

THE EFFECT OF PROJECTILE SHAPE ON THE BALLISTIC PERFORATION OF THIN METAL PLATES

MAJ. THOMAS E. FIELDS

FOREWORD

This report is based on a thesis prepared by Major Thomas E. Fields of the Air Force Institute of Technology as partial fulfillment of requirements for the degree of Master of Science. The work was administered by Mr. Gordon H. Griffith of the Air Force Materials Laboratory under Project 7360, "Chemistry and Physics of Materials", Task 736006, "Response of Materials to Impulsive Loading".

The author gratefully acknowledges the assistance of Major Ronald Prater of the Air Force Materials Laboratory and members of the staff of the University of Dayton Research Institute, particularly Mr. Hallock F. Swift and Mr. Diamantis D. Preonas, for their pertinent advice, guidance and encouragement, and Mr. Michael Lehman, Mr. James Green, Mr. Lewis A. Shiverdecker, and Mr. Edward A. Strader for their technical assistance and support under Contract F33615-68-C-1138, Response of Materials to Pulse Loads. The author also wishes to thank his AFIT faculty committee, headed by Dr. Delmar W. Breuer, and his thesis advisor, Major William Goldberg, for their counsel and help in completing this report.

The manuscript was released by the author in June 1969 for publication.

This technical report has been reviewed and is approved.

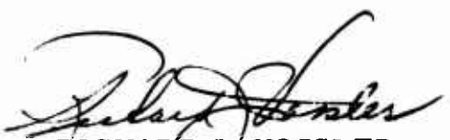

RICHARD J. VOSSLER
Chief, Exploratory Studies Branch
Materials Physics Division
AF Materials Laboratory

ABSTRACT

The effect of projectile shape on thin target perforation was investigated for five projectile shapes impacting aluminum and steel targets at 506 m/sec. A discarding sabot technique was developed for launching the unjacketed steel projectiles and accurate perforation velocity losses were measured using a ballistic pendulum with the targets mounted in the center of the pendulum. The five projectile shapes included two pointed ogives, a shape similar to a Russian 14.5 mm AP core, a cylinder and a cone. The two ogive shapes were the most efficient penetrators while the velocity loss of the Russian projectile averaged 15% higher. The cone, which caused a combined petaling and plugging target failure, was the least effective shape. Calculations with two approximate perforation theories predicted smaller velocity losses than were found experimentally.

Contents

Contents (Continued)

List of Figures

List of Figures (Continued)

List of Tables

I. Introduction

One major engineering problem in weapon system design has been the limited basic research in penetration mechanics. Although a large body of empirical knowledge has been collected, a satisfactory model to explain the complicated mechanisms of penetration and perforation has not been developed. The subject of ballistic perforation of thin targets is of particular interest to the Air Force in the design of aircraft armor and armament. Simplified theories for the deformation and failure of thin plates have generally led to mathematical equations relating projectile size and shape; target strength and thickness; and the impact velocity. The purpose of this study is to investigate the effect of projectile shape on the perforation of thin aluminum and steel plates. The variation of projectile velocity with nose shape during normal impact at ballistic velocities is the primary area of interest.

Background

Penetration is defined as the entry of a missile into a target without completing its passage through the target, while perforation is

the complete passage of the missile through the target (Ref 19:198). Plate perforation appears to involve the simultaneous action of crack formation, spalling, elastic and plastic wave propagation, friction and heating, and perhaps shattering of the projectile (Ref 9:241). Failure

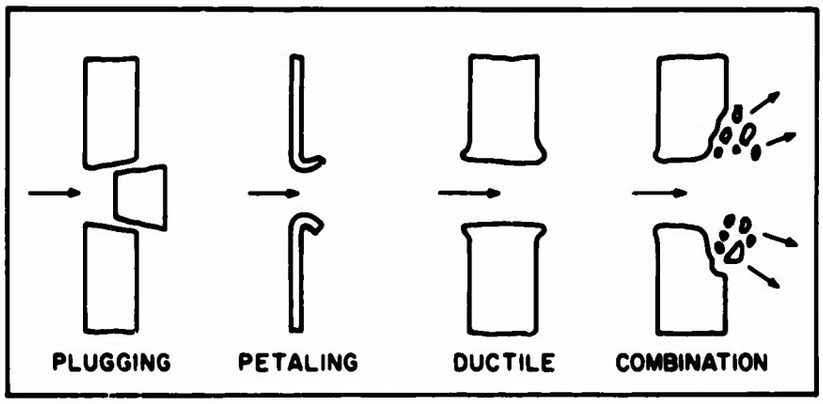

Fig. 1. Common Types of Plate Failure (From Ref 19:206-207)

of the plate is usually a combination of the four types shown in Fig. 1, with one of the mechanisms predominating (Ref 19:206-207). Plugging is most common in plates of moderate thickness while petaling usually occurs in thin plates impacted at velocities less than 3,000 ft/sec. At higher velocities, thin plates generally fail by plugging. The two modes, ductile failure, or the combination of ductile failure and spalling, are characteristic of thick plates of medium or low hardness. While a complete analysis of all perforation mechanisms is impractical, several simplified models have been proposed for specific failure modes.

Survey of Perforation Models

The works of Bethe (Ref 2) and Taylor (Ref 23), based on a ductile type failure, describe the enlargement of a circular hole in a

thin plastic sheet. These analyses consider the equilibrium elastic and plastic stress distribution in an infinite sheet pierced by a pointed conical projectile. Freiberger (Ref 6) extended these studies to include target inertia effects in the equilibrium equations. Another approach to the ductile model considered the analogy between a plastic membrane and a thin flexible wire (Ref 4).

Other theories for thin plate perforation have been derived from momentum considerations. One analysis proposed for a petaling or dishing deformation pattern is based on the assumption that the inertia forces are much greater than the material strength, a good approximation at high projectile velocities (Ref 26). Nishiwaki (Ref 17) derived an expression relating the momentum of the displaced target material to the pressure exerted on the target by the projectile. This theory assumes that the target deformation conforms to the shape of the projectile and that target yielding occurs under a constant static pressure which can be determined from static tests. Several models for thin plate failure by plugging have been proposed which relate the projectile velocity change to the plug momentum and the energy required to shear the plug from the target (Refs 8, 9, 21).

A quasi-dynamical approach by Thomson (Ref 24) considers the energy dissipated by plastic work in displacing the target material, the acceleration of the particles in the displaced material, and the heat produced by friction. This analysis, an extension of the Taylor hole enlargement theory, assumes a dish type perforation pattern.

Purpose

Each of these approximate theories depends on projectile shape either directly or through an assumed type of target failure. The purpose of this study is to experimentally measure the velocity losses for several projectile shapes perforating thin aluminum and steel targets. The measured losses will be compared with values calculated from the models proposed by Thomson and Nishiwaki. A more complete development of these theories is given in the succeeding section.

II. Theory

The approximate perforation theories of Thomson and Nishiwaki were used to calculate predicted projectile velocity losses for comparison with the experimental values.

Thomson Theory (Ref 24)

This theory is a quasi-dynamical analysis of the circular hole enlargement theory proposed by Taylor (Ref 23). An unsymmetric dish type perforation pattern (Fig. 2) is assumed for the two-dimensional problem in which the plate thickness is small compared to the hole diameter. The projectile is assumed to perforate the plate at constant velocity without shattering. In his analysis, Thomson derives analytical expressions for the energy dissipated in plastic deformation of the target, acceleration of the displaced target material and friction heating. This derivation assumes that the radial and axial stresses in the crater are zero and that plastic yielding occurs at constant volume with the circumferential stress equal to the yield stress.

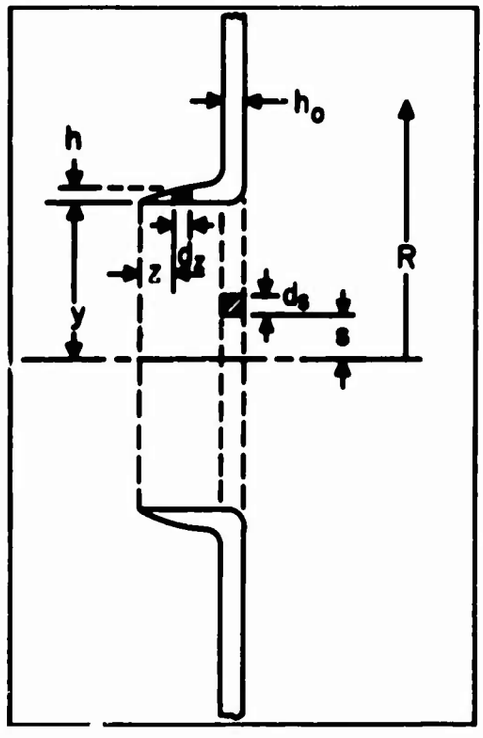

Fig. 2. Unsymmetric Perforation (From Ref 24:80)

For the pattern shown in Fig. 2, the plastic work per unit volume to deform an elemental ring, ds, is given by:

$$\frac{W_p}{\text{volume}} = \int_0^{\varepsilon_{\theta/y}} \sigma_y d\varepsilon_\theta = \sigma_y \varepsilon_{\theta/y} \tag{1}$$

where ε_θ is the circumferential strain; $\varepsilon_{\theta/y}$ is the strain at $s = y$; and σ_y is the target yield stress. But $\varepsilon_{\theta/y}$ is:

$$\int_s^y \frac{2\pi ds}{2\pi s} = \ln\left(\frac{y}{s}\right) \tag{2}$$

The work now becomes:

$$\frac{W_p}{\text{volume}} = \sigma_y \ln\left(\frac{y}{s}\right) \tag{3}$$

For the volume, $2\pi h_o s ds$, the work performed on the ring is:

$$W_p = 2\pi \sigma_y h_o s \ln\left(\frac{y}{s}\right) ds \tag{4}$$

For all such rings, the plastic work is:

$$W_p = \int_0^y 2\pi h_o \sigma_y s \ln\left(\frac{y}{s}\right) ds = \frac{\pi y^2 h_o \sigma_y}{2} \tag{5}$$

As the maximum projectile radius, R, intersects the target face, plastic deformation is complete and the total work is:

$$W_p = \frac{\pi R^2 h_o \sigma_y}{2} \tag{6}$$

In calculating the dynamic work required to radially accelerate the target crater material, the target is assumed to be at rest. The accelerating force is then given by:

$$F = M\frac{d^2y}{dt^2} + \frac{dM}{dt}\frac{dy}{dt} \tag{7}$$

The displaced target mass, M, is $\pi\rho h_o y^2$ and the dynamic work is:

$$W_d = \int_o^r M\frac{d^2y}{dt^2}\,dy + \int_o^r \frac{dM}{dt}\frac{dy}{dt}\,dy \tag{8}$$

or

$$W_d = \pi\rho h_o\left[\int_o^r y^2\frac{d^2y}{dt^2}\,dy + 2\int_o^r y\left(\frac{dy}{dt}\right)^2 dy\right] \tag{9}$$

where r is the hole size at any time t and ρ is the target mass density. From the constant velocity assumption and the geometry shown in Fig. 3, the derivatives can be expressed as:

$$\frac{dy}{dt} = v\frac{dy}{dx} \qquad \text{and} \qquad \frac{d^2y}{dt^2} = v^2\frac{d^2y}{dx^2} \tag{10}$$

where v is the impact velocity. The dynamic work for complete projectile perforation now becomes:

$$W_d = \pi\rho h_o v^2\left[\int_o^R y^2\frac{d^2y}{dx^2}\,dy + 2\int_o^R y\left(\frac{dy}{dx}\right)^2 dy\right] \tag{11}$$

From a study of the friction work, Thomson concludes that the energy dissipated in heating the projectile target interface can be neglected. The total perforation work then becomes the sum of the plastic and dynamic work.

$$W = \frac{\pi R^2 h_o \sigma_y}{2} + \pi\rho h_o v^2\left[\int_o^R y^2\frac{d^2y}{dx^2}\,dy + 2\int_o^R y\left(\frac{dy}{dx}\right)^2 dy\right] \tag{12}$$

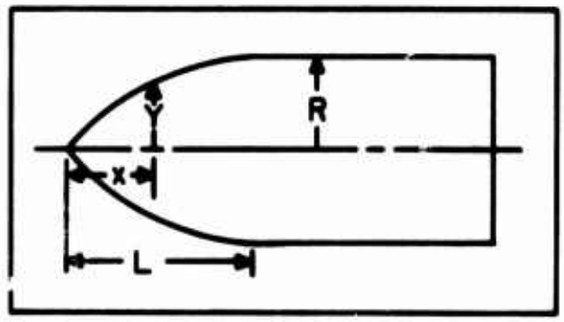

Fig. 3. Projectile Dimensions (From Ref 24:81)

In calculating the residual velocity, the perforation work was equated to the change in linear kinetic energy from the relation:

$$\frac{1}{2}mv^2 - \frac{1}{2}mv_r^2 = W \tag{13}$$

where v_r is the residual velocity and m is the projectile mass. From Equations 12 and 13, the residual velocity is:

$$v_r^2 = v^2\left\{1 - \frac{2\pi\rho h_o}{m}\left[\int_o^R y^2\frac{d^2y}{dx^2}\,dy + 2\int_o^R y\left(\frac{dy}{dx}\right)^2 dy\right]\right\} - \frac{\pi R^2 h_o \sigma_y}{m} \tag{14}$$

With appropriate projectile and target parameters, Equation 14 can be solved for the theoretical perforation velocity loss.

Nishiwaki Theory (Ref 17)

Nishiwaki proposed an expression relating the momentum of the target crater material to the total pressure exerted on the projectile by the target. He assumes that the displaced target material remains in contact with the projectile nose and that yielding occurs at a pressure equal to the dynamic pressure plus a constant static component P_o,

which can be determined from static tests. For the projectile shown in Fig. 4, the normal and friction forces acting on an incremental surface element dA, are:

$$F_n = P_o \qquad \text{and} \qquad F_f = \mu P_o \tag{15}$$

where μ is the coefficient of static friction. The resistance to a projectile moving slowly through the target is then given by:

$$dR_o = P_o dA(\sin \alpha + \mu \cos \alpha) \tag{16}$$

For a sufficiently large projectile velocity, the displacement of target material in contact with the projectile is assumed to be normal to the contact surface with a velocity equal to the component of the projectile velocity in this direction. The momentum of the material displaced per unit time is:

$$(\rho v\, dA) \sin \alpha \cdot v \sin \alpha \tag{17}$$

where ρ is the target density and v is the projectile velocity. The dynamic pressure is therefore equal to $\rho v^2 \sin^2 \alpha\, dA$. To obtain the resistance to projectile motion, P_o is replaced by the sum of the static and dynamic pressures and a coefficient of kinetic friction μ_K, used in place of μ.

$$dR = (P_o + \rho v^2 \sin^2 \alpha)\, dA\, (\sin \alpha + \mu_K \cos \alpha) \tag{18}$$

Neglecting the friction term, the equation of motion for a projectile of mass M, is:

$$M \frac{dv}{dt} = -\int_A (P_o + \rho v^2 \sin^2 \alpha) \sin \alpha\, dA \tag{19}$$

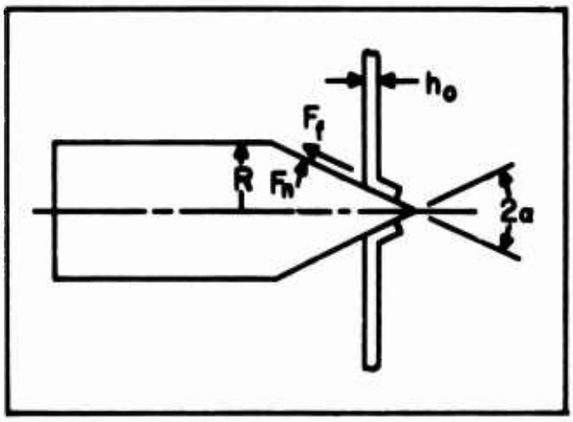

Fig. 4. Nishiwaki Model

For the conical shape, Equation 19 can be integrated in three steps to give:

$$v_r^2 = \left(v^2 + \frac{P_o}{\rho \sin^2 \alpha}\right) e^{-\frac{2\pi\rho R^2 h_o \sin^2 \alpha}{M}} - \frac{P_o}{\rho \sin^2 \alpha} \qquad (20)$$

where v_r is the residual velocity.

The static pressure, assumed constant for a given target material and thickness, can be calculated for aluminum from the equation:

$$P_o = 5.4\, h_o \ \text{kg/mm}^2 \qquad (21)$$

where the numerical constant was determined from static perforation tests on several thicknesses of aluminum plates. To apply Equation 21 to steel targets, the following relation between pressure and target properties was assumed.

$$P_o = \frac{k h_o \sigma_y}{d} \tag{22}$$

where k is a proportionality constant and d is the maximum projectile diameter. For equal values of d, Equations 21 and 22 give:

$$P_o = \frac{5.4\, h_o \sigma_{y(\text{steel})}}{\sigma_{y(\text{aluminum})}} \tag{23}$$

The assumptions made in the Thomson and Nishiwaki models neglect several perforation phenomena which may cause appreciable projectile energy losses. Neither theory considers the energy dissipated in elastic and plastic wave propagation, target crack formation or projectile deformation. Modes of target failure not considered by the models have been observed in experimental tests. Greater projectile energy losses would be expected for the more complex deformation patterns.

Kucher Optimal Shape (Ref 13)

Using Thomson's energy theory, Kucher applied normal optimization techniques to find a projectile shape which minimized the energy dissipated in dynamical work. This shape, described by the equation

$$y = R \left(\frac{x}{L}\right)^{3/4} \tag{24}$$

was used as one of the experimental shapes in this study.

Projectile Spin

The use of spin stabilized projectiles in this study was based on an assumption that spin effects are negligible in thin target perforation. The validity of this assumption is supported by the results of previous theoretical and experimental analyses. In his study of perforation work, Thomson (Ref 24) concluded that a molten projectile target interface exists during perforation and that frictional losses are quite small compared to other energy losses. From experimental measurements of the forces resisting penetration by a spinning projectile, Krafft (Ref 12) found evidence which supports the molten interface theory. His results indicate that sliding friction accounts for less than 3% and possibly less than 1% of the projectile striking energy.

III. Experimental Procedure

The five projectile shapes used in this study were the "Ogive", "Russian", "Optimal", "Cone" and "Cylinder". A comparison of the shapes is shown in Fig. 5. The Ogive shape is the same as the core of a standard U. S. .50 caliber armor piercing bullet while the Russian nose was patterned from the core of a Russian 14.5 mm armor piercing bullet (Ref 3). Kucher's equation of an optimal penetrator for thin plates was used for the Optimal nose. The Cone is a right circular cone with a 45 degree semi-vertex angle and the Cylinder is a flat-ended right circular cylinder. The diameter of the projectiles was 1.11 $\pm$ 0.01 cm. A description of the projectiles, including lengths, average masses and sabots, is given in Appendix B. While it was desirable to have all projectiles equal in mass, variations between the different shapes were required for aerodynamic stability. The average masses ranged from 18.59 gm for the Optimal shape to 19.88 gm for the Cylinder with a maximum deviation within a single shape of 0.46 gm.

A muzzle velocity of 531 m/sec was selected to obtain the largest velocity change during target perforation consistent with projectile stability requirements. To achieve this velocity, a constant load of 5.31 gm of Dupont IMR 4064 powder was used for all data shots. Since this load did not completely fill the cartridge, two cloth cleaning patches were used to fill the void. A uniform projectile seating depth was obtained by crimping the cartridge neck into the sabot crimping

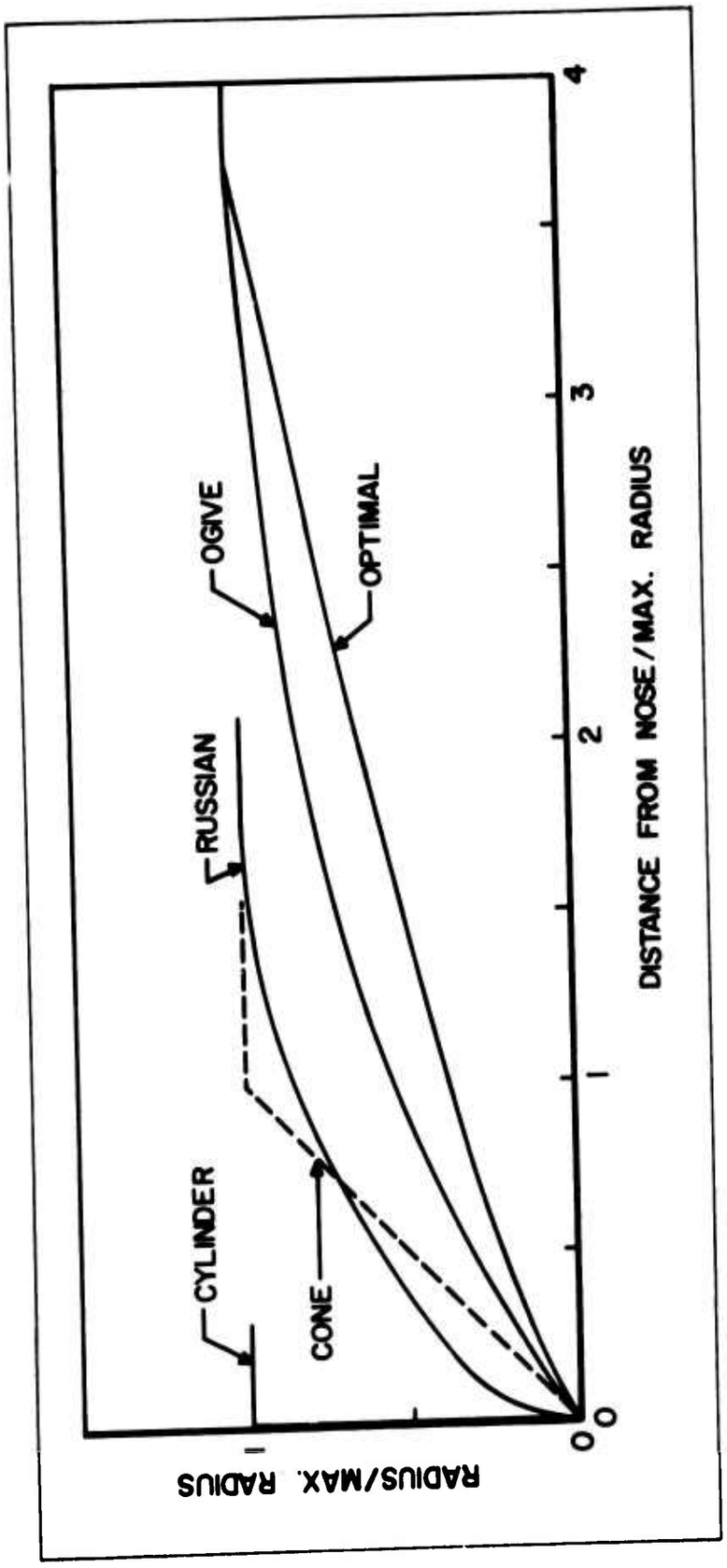

Fig. 5. Comparison of Projectile Nose Shapes

ring. The average muzzle velocity of the test series was 514.74 m/sec with a maximum deviation of 37.18 m/sec. Velocity variations were due to differences in projectile mass and non-uniform gas leakage around the sabots.

Preliminary calculations using the Thomson theory predicted very small differences in perforation velocity loss between the different shapes. To achieve the accurate measurements necessary for comparing the five projectile shapes, a symmetric ballistic pendulum was used to measure the velocity losses (Fig. 6). The pendulum was designed to contain all target debris except particles near the trajectory centerline and pendulum accuracy was achieved through the use of a suspension length which was very large compared to the length of the pendulum half swing. A suspension length of 243.84 cm was used while the maximum pendulum half swing for the data shots was 4.404 cm. Photographs of the pendulum displacement was used to calculate the projectile momentum loss, assuming a constant projectile mass. The pendulum, range layout and other equipment are described in detail in Appendix A and Appendix C outlines the pendulum alignment and calibration procedures. The projectile velocity prior to target impact was calculated from a measurement of the time to traverse the measured distance between the initial velocity switches. Residual projectile velocities and target plug velocities were determined from two timed x-ray photographs taken down range of the pendulum. The target plugs were stopped in five layers of 3.8 cm thick Celetex board placed inside the catch tank. The plug momentum

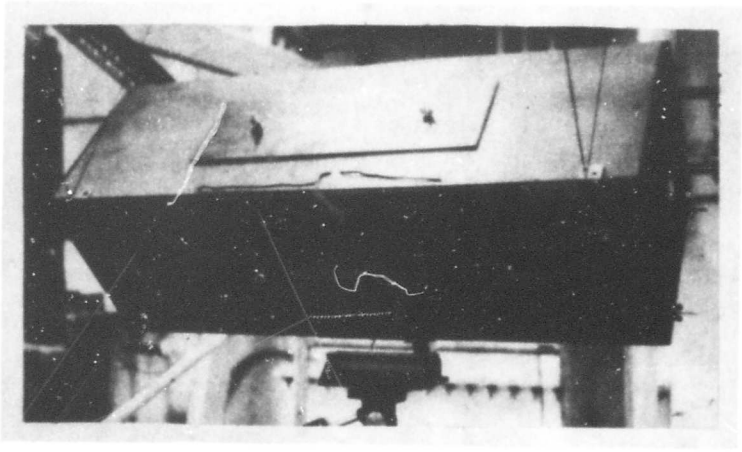

Fig. 6. Ballistic Pendulum

was calculated from the recovered plug mass and the x-ray velocity. Sample data calculations are given in Appendix D.

IV. Results and Discussion

Results

Tables I through IV list the experimental results for the five projectile shapes by target material and thickness. The tabulation includes projectile mass, target impact velocity and perforation velocity loss. Ratios of velocity loss to impact velocity and linear kinetic energy loss to impact energy are also given. A plot of the velocity ratios against target thickness is shown in Fig. 7. Since only three target thicknesses were used, the data points were spread about the ordinate for ease of reading. The upper part of the graph shows data for steel targets, while aluminum target data is shown on the lower portion.

Discussion

The average impact velocity for the 44 data shots was 506.27 m/sec with a maximum deviation of 60.90 m/sec. Velocity variations were attributed to differences in projectile mass and gas leakage around the sabots. With the exception of Cylinder shots through steel, no permanent projectile deformation was detected. Against steel, the impact end of the Cylinder flattened, shearing a target plug approximately 10% larger than the projectile diameter. For other shapes, the target hole and projectile diameters were essentially the same.

There were two basic target perforation patterns, petaling and plugging, for the five projectile shapes. Petal craters were formed by

Table I

Results for 0.159 cm 6061-T6 Aluminum Targets

Shape	Shot No.	Mass (gm)	Impact Velocity V_o (m/sec)	Perforation Velocity Loss ΔV (m/sec)	$\frac{\Delta V}{V_o}$	$\frac{\Delta E}{E_o}$
Ogive	2	19.34	535.59	7.22	0.0135	0.0268
Ogive	3	19.25	529.74	6.98	0.0132	0.0262
Optimal	4	19.35	517.70	7.19	0.0139	0.0276
Optimal	5	19.37	518.77	7.16	0.0138	0.0274
Russian	7	19.73	507.98	12.34	0.0243	0.0480
Russian	57	19.75	499.35	12.53	0.0251	0.0495
Cone	9	19.70	507.19	14.69	0.0290	0.0571
Cone	10	19.71	515.45	14.81	0.0287	0.0566
Cylinder	58	19.89	476.01	13.75	0.0289	0.0569
Cylinder	59	19.88	508.98	11.46	0.0225	0.0445

Table II

Results for 0.317 cm 6061-T6 Aluminum Targets

Shape	Shot No.	Mass (gm)	Impact Velocity V_o (m/sec)	Perforation Velocity Loss ΔV (m/sec)	$\frac{\Delta V}{V_o}$	$\frac{\Delta E}{E_o}$
Ogive	13	19.39	485.73	23.07	0.0475	0.0927
Ogive	14	19.32	489.45	24.14	0.0493	0.0962
Ogive	56	19.28	555.89	20.57	0.0370	0.0726
Optimal	12	19.31	518.56	22.77	0.0439	0.0859
Optimal	15	19.59	521.30	24.72	0.0474	0.0926
Optimal	16	19.24	528.25	24.66	0.0467	0.0912
Optimal	19	19.41	519.90	23.10	0.0444	0.0869
Optimal	41	18.59	497.37	24.35	0.0490	0.0955
Russian	23	19.82	528.37	24.60	0.0466	0.0909
Russian	25	19.80	497.95	26.43	0.0531	0.1033
Cone	22	19.78	531.39	32.49	0.0611	0.1185
Cone	24	19.82	505.97	30.05	0.0594	0.1152
Cylinder	26	19.87	480.97	26.61	0.0553	0.1076
Cylinder	27	19.89	480.82	27.92	0.0581	0.1128

Table III

Results for 0.476 cm 6061-T6 Aluminum Targets

Shape	Shot No.	Mass (gm)	Impact Velocity V_o (m/sec)	Perforation Velocity Loss ΔV (m/sec)	$\frac{\Delta V}{V_o}$	$\frac{\Delta E}{E_o}$
Ogive	28	19.32	529.74	36.06	0.0681	0.1315
Ogive	29	19.28	520.17	38.31	0.0736	0.1419
Optimal	39	18.29	488.99	41.18	0.0842	0.1613
Optimal	40	18.82	526.15	35.84	0.0681	0.1316
Russian	31	19.79	503.99	41.27	0.0819	0.1571
Russian	42	19.24	496.21	42.49	0.0856	0.1639
Cone	32	19.79	512.58	52.21	0.1018	0.1933
Cone	33	19.69	520.32	48.16	0.0926	0.1765
Cone	43	19.92	472.10	50.32	0.1066	0.2018
Cone	55	19.76	514.81	51.51	0.1011	0.1901
Cylinder	34	19.87	497.55	44.84	0.0901	0.1721
Cylinder	36	19.88	489.23	44.84	0.0916	0.1749

Table IV

Results for 0.317 cm 1030 Steel Targets

Shape	Shot No.	Mass (gm)	Impact Velocity V_o (m/sec)	Perforation Velocity Loss ΔV (m/sec)	$\frac{\Delta V}{V_o}$	$\frac{\Delta E}{E_o}$
Ogive	54	19.27	509.47	49.86	0.0979	0.1861
Optimal	50	18.66	507.61	48.07	0.0947	0.1804
Russian	49	19.20	486.09	57.70	0.1187	0.2233
Russian	53	19.81	490.30	61.11	0.1246	0.2337
Cone	47	19.90	491.22	73.09	0.1488	0.2754
Cone	48	19.73	521.24	73.03	0.1401	0.2606
Cylinder	44	19.88	445.37	93.45	0.2098	0.3756
Cylinder	46	19.90	494.08	99.85	0.2021	0.3633

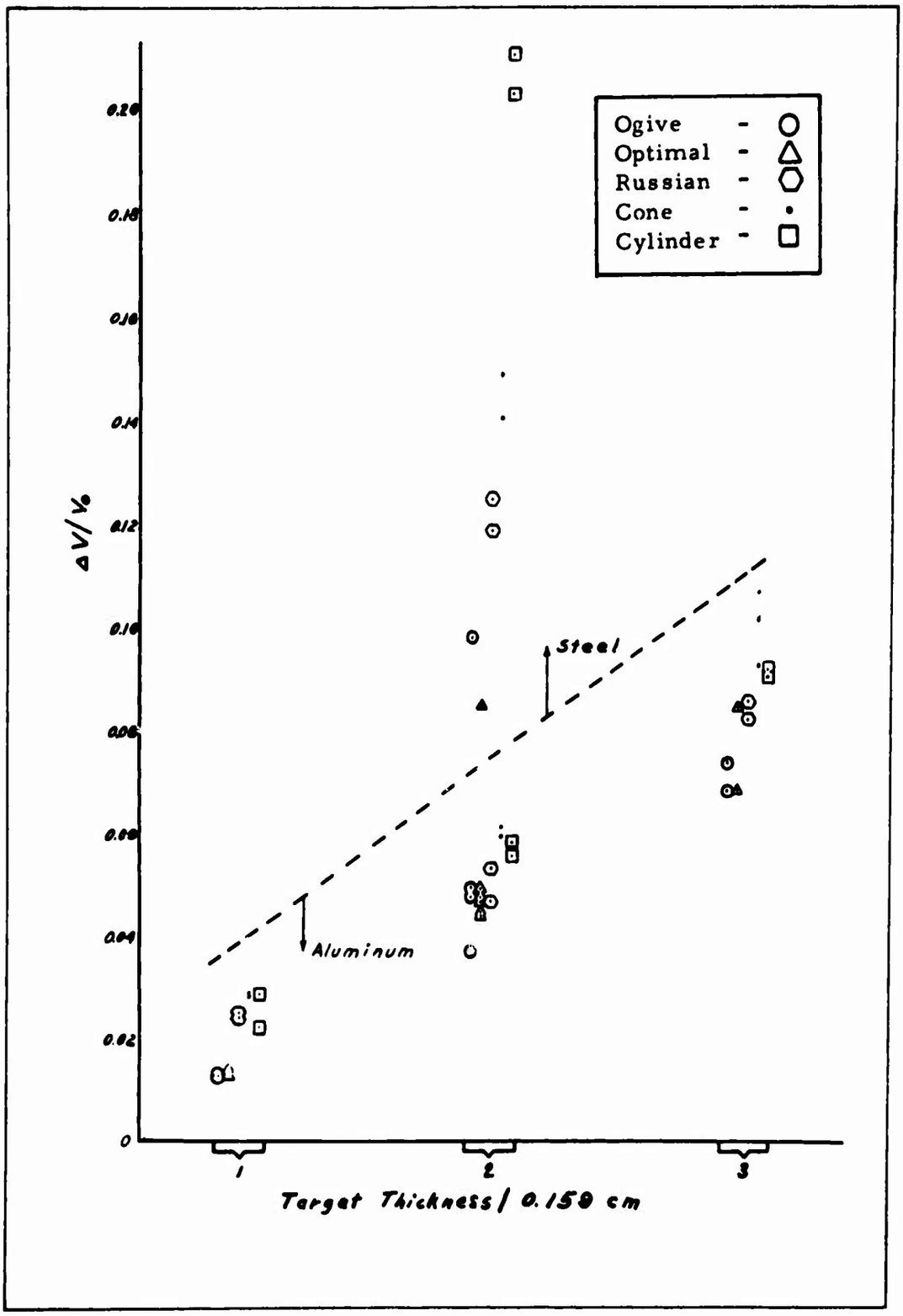

Fig. 7. Projectile Velocity Loss

the Ogive and Optimal shapes while the Cone and Cylinder shapes plugged the target. The Cylinder plugs were flat discs with a nearly uniform thickness equal to the target thickness, indicating negligible target yielding prior to shear failure. Small spherical depressions in the center of the impact face of the plugs were probably caused by a compressed air pocket at the projectile target interface. The Cone plugs were cratered in a conical shape, with the thickness varying from zero at the crater vertex to the target thickness at the outside shear face. Petal cracks in the crater indicated ductile target yielding prior to failure. The Russian projectiles caused target petaling but on each shot, one or more of the petals fractured from the target and were found in the pendulum liner. All detectable target debris, other than trajectory plugs, was contained in the ballistic pendulum.

The experimental error for the projectile velocity losses measured with the pendulum was 1.6%. For the Cones and Cylinders, a decreased accuracy of 3.8% resulted from additional measurements of the plug momentum. To verify test data, multiple shots were fired into each target. For the aluminum targets, two tests were conducted with each projectile shape, while additional shots with selected shapes were used to determine data reproducibility. Although the projectile mass and velocity variation between data shots precludes a direct quantitative comparison of different shapes, some qualitative conclusions can be made. In this comparison, the ratio of the residual to impact velocity was taken as a measure of the perforation effectiveness.

Ogive and Optimal Shapes. With the overlap in perforation data for these projectiles, neither shape can be established as the more efficient penetrator. In general, the slender pointed Ogive and Optimal shapes appear to be more effective than the blunter noses of the other projectiles. Aerodynamic instability after target perforation was a problem with both projectiles during data tests. On shots against the 0.317 cm and 0.476 cm targets, projectile yaw angles up to ninety degrees from trajectory were found in the x-ray photographs. Two Optimal shots struck the rear end plate of the pendulum and the data had to be discarded. A modification on the remaining Optimal projectiles moved the mass center forward, providing improved stability on subsequent firings.

Russian Shape. While these projectiles lost more velocity in target perforation than either the Ogive or Optimal shapes, the relative effectiveness of the Russian shape increased with target thickness. The energy required for initial hole formation by the blunt nose may account for most of the difference between this projectile and the pointed shapes. The Russian projectiles were the most aerodynamically stable of the five shapes, with no observed deviation from trajectory on any test shot.

Cones and Cylinders. Of the five shapes tested, the Cone was the least effective p[illegible]or aluminum targets. Target failure for both the Cylinder and Cone was by plugging with the Cylinder plugs leaving the target at a velocity greater than the projectile, while the

Cone plugs remained in contact with the projectile nose. The larger velocity loss of the Cones probably resulted from the additional energy expended in deforming the target prior to plug failure.

To obtain a measure of the relative performance of the projectile shapes, average values of the ratios of energy loss to impact energy were calculated for each shape and target thickness. These averages which are plotted against the three aluminum target thicknesses in Fig. 8, show the general effect of shape in target perforation.

The Thomson and Nishiwaki theories were used to calculate predicted residual velocities for comparison with the test data. The projectile shape equations, required in these calculations, were known for each of the shapes except the Ogive and Russian. To obtain expressions for these shapes, coordinates of points along the nose curves were measured and key punched on IBM data cards with the Automatic Film Reader described in Appendix A. An IBM 7094 computer was used to fit least squares polynomial curves to the coordinate data. Attempts to fit the Russian shape resulted in second and third order curves with large deviations from the true shape, and higher order polynomials which contained irregular curve reversals between data points. A good approximation to the Ogive shape, with a maximum deviation of 0.27 mm, is given by:

$$y = 0.0191472\, x^3 - 0.193018\, x^2 + 0.719882\, x + 0.00661773 \qquad (25)$$

A plot of this curve and the input coordinates is shown in Fig. 9.

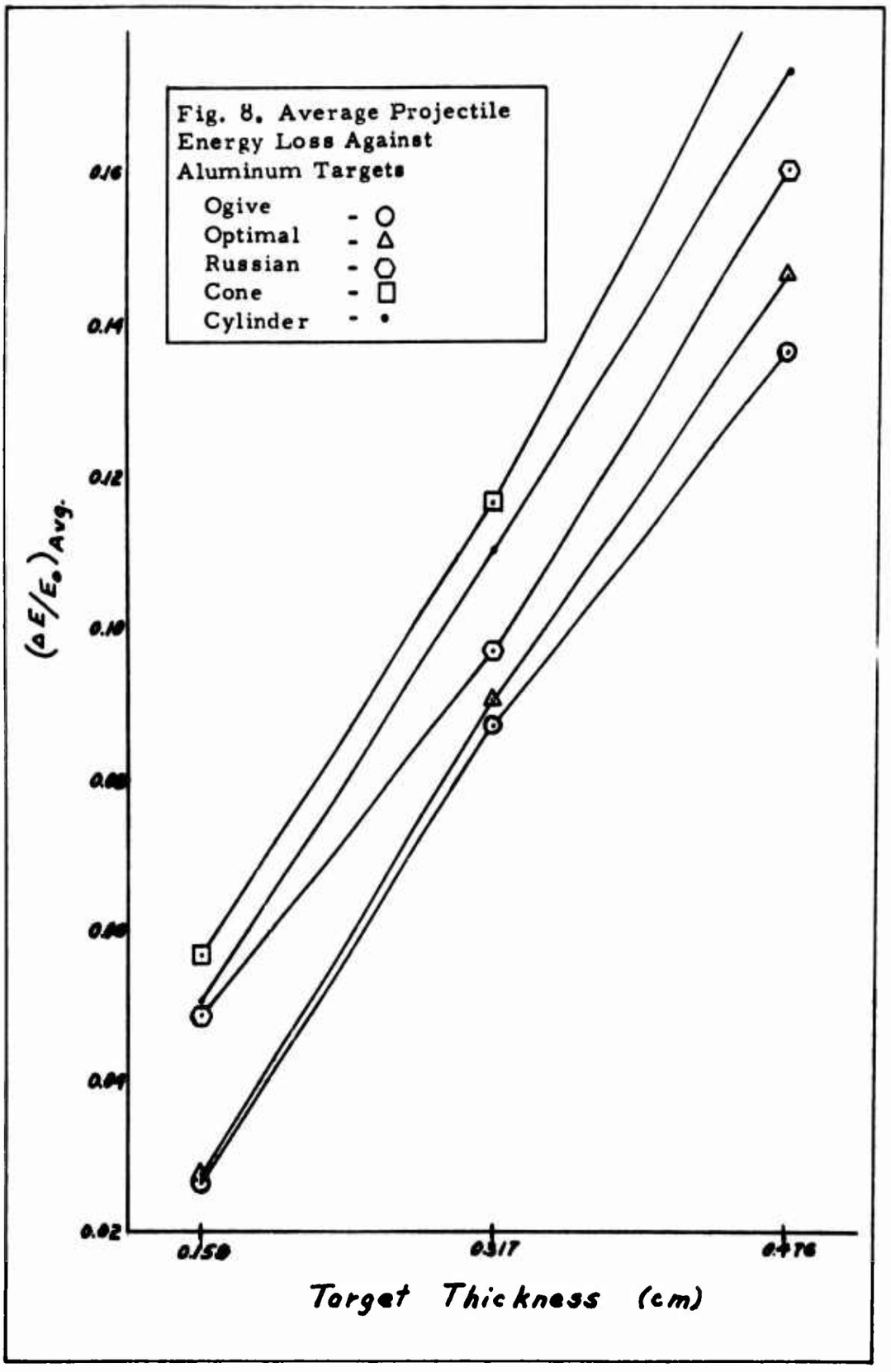
Fig. 8. Average Projectile Energy Loss Against Aluminum Targets
Ogive - ○
Optimal - △
Russian - ⬡
Cone - □
Cylinder - •
0.16
0.14
0.12
0.10
0.02
$(\Delta E/E_o)_{Avg.}$
0.158
0.317
0.476
Target Thickness (cm)

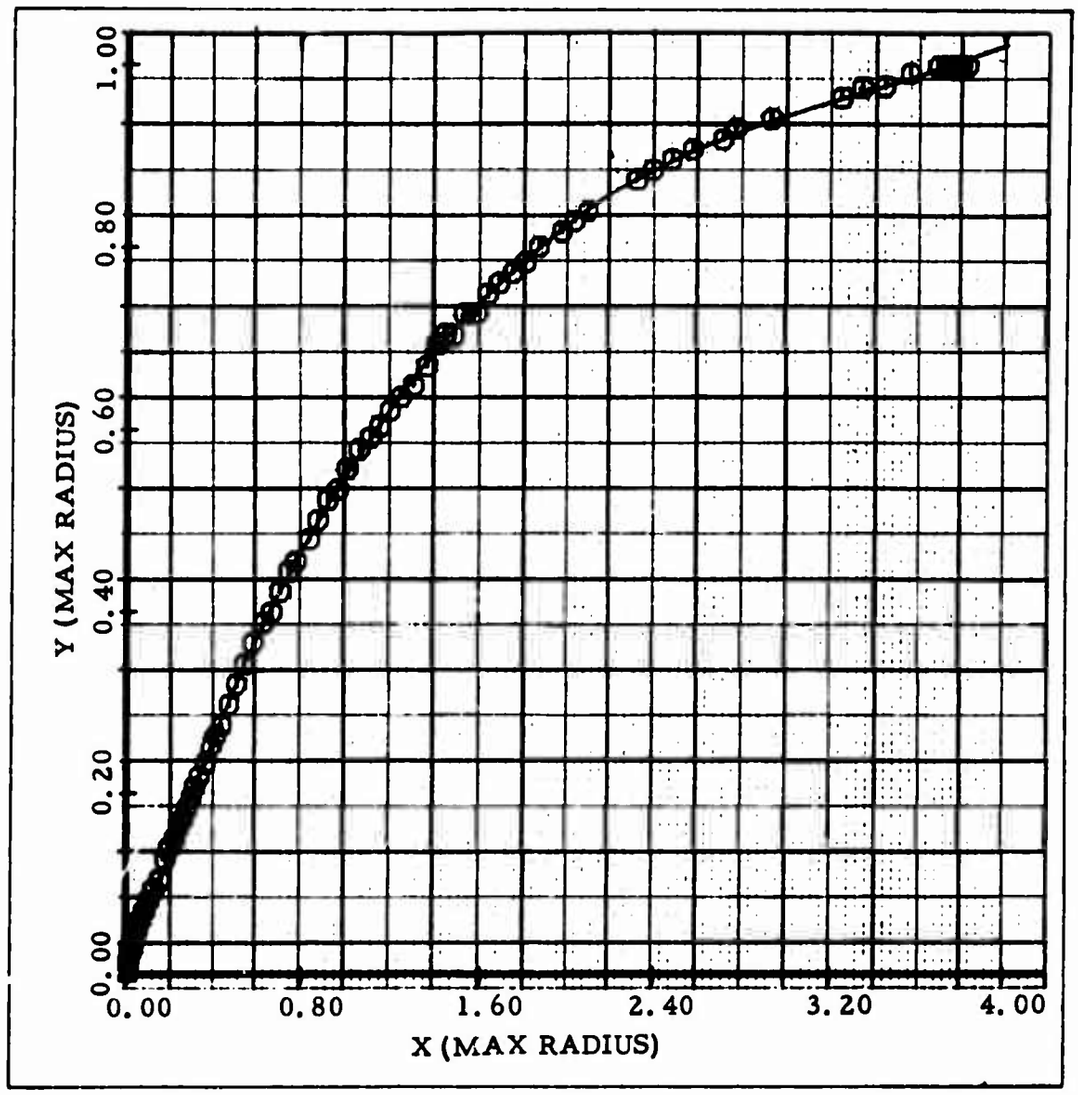

Fig. 9. Polynomial Curve Fit for Ogive

Velocity losses for the Ogive, Optimal and Cone shapes were calculated from the Thomson energy theory while the Nishiwaki theory was used in calculations for the Cone and Cylinder shapes. Theoretical velocity losses were not computed for the Russian projectiles since the equation of the nose shape was unknown. The target yield stresses used in the calculations were 27.58×10^8 dynes/cm^2 for aluminum and 34.47×10^8 dynes/cm^2 for steel (Ref 3).

Tables V-VIII list the theoretical and experimental data by target type and thickness and Figs. 10-13 show a comparison of the theory for each projectile shape against aluminum targets. Both theories predict lower velocity losses than were found experimentally. This disparity increased with target thickness and was much larger in the steel target calculations. In general, the Nishiwaki theory provides closer agreement to the data with differences which vary little with projectile shape but appear to depend on target thickness and material. The most logical term in the Nishiwaki model to account for this type of variation is P_o which was determined from static tests. Since this method neglects the increase in target resistance during dynamic perforation, a better approximation to the data should be obtained with a value of P_o corrected for dynamic effects. This dynamic pressure should be a function of the static yield pressure, target thickness and impact velocity. Two possible forms are:

$$P_d = k P_o h_o v_o \qquad \text{or} \qquad P_d = k P_o h_o v_o^2 \tag{26}$$

The value of k would have to be determined from the experimental data. The differences between the Thomson theory and experimental data for the cone shape are not representative since target failure by plugging was not considered in the theoretical model. For the Ogive and Optimal shapes, the differences between theory and experiment appear to vary with both projectile shape and target properties. The use of a dynamic yield stress in the Thomson equation should provide better overall

Table V

Comparison of Theoretical Velocity Losses
for Shots Against 0.159 cm 6061-T6 Aluminum Targets

Experimental Data					Thomson Theory	Nishiwaki Theory
Shape	Shot No.	Mass (gm)	Impact Velocity (m/sec)	Velocity Loss - Δv (m/sec)	Velocity Loss - Δv (m/sec)	Velocity Loss - Δv (m/sec)
Ogive	2	19.34	535.59	7.22	2.76	-
Ogive	3	19.25	529.74	6.98	2.79	-
Optimal	4	19.35	517.70	7.19	2.71	-
Optimal	5	19.37	518.77	7.16	2.70	-
Cone	9	19.70	507.19	14.69	2.93	10.89
Cone	10	19.71	515.45	14.81	2.91	11.05
Cylinder	58	19.89	476.01	13.75	-	10.11
Cylinder	59	19.88	508.98	11.46	-	10.78

Table VI

Comparison of Theoretical Velocity Losses
for Shots Against 0.317 cm 6061-T6 Aluminum Targets

Experimental Data					Thomson Theory	Nishiwaki Theory
Shape	Shot No.	Mass (gm)	Impact Velocity (m/sec)	Velocity Loss - Δv (m/sec)	Velocity Loss - Δv (m/sec)	Velocity Loss - Δv (m/sec)
Ogive	13	19.39	485.73	23.07	5.82	-
Ogive	14	19.32	489.45	24.14	5.82	-
Ogive	56	19.28	555.89	20.57	5.45	-
Optimal	12	19.31	518.56	22.77	5.44	-
Optimal	15	19.59	521.30	24.72	5.35	-
Optimal	16	19.24	528.25	24.66	5.40	-
Optimal	19	19.41	519.90	23.10	5.40	-
Optimal	41	18.59	497.37	24.35	5.79	-
Cone	22	19.78	531.39	32.49	5.73	22.42
Cone	24	19.82	505.97	30.05	5.85	21.29
Cylinder	26	19.87	480.97	26.61	-	20.17
Cylinder	27	19.89	480.82	27.92	-	20.12

Table VII

Comparison of Theoretical Velocity Losses
for Shots Against 0.476 cm 6061-T6 Aluminum Targets

Experimental Data					Thomson Theory	Nishiwaki Theory
Shape	Shot No.	Mass (mg)	Impact Velocity (m/sec)	Velocity Loss - Δv (m/sec)	Velocity Loss - Δv (m/sec)	Velocity Loss - Δv (m/sec)
Ogive	28	19.32	529.74	36.06	8.38	-
Ogive	29	19.28	520.17	38.31	8.48	-
Optimal	39	18.29	488.99	41.18	8.95	-
Optimal	40	18.82	526.15	35.84	8.32	-
Cone	32	19.79	512.58	52.21	8.76	32.06
Cone	33	19.69	520.32	48.16	8.74	32.66
Cone	43	19.92	472.10	50.32	9.06	29.33
Cone	55	19.76	514.81	51.51	8.75	32.20
Cylinder	34	19.87	497.55	44.84	-	30.05
Cylinder	36	19.88	489.23	44.84	-	30.43

Table VIII

Comparison of Theoretical Velocity Losses
for Shots Against 0.317 cm 1030 Steel Targets

Experimental Data					Thomson Theory	Nishiwaki Theory
Shape	Shot No.	Mass (gm)	Impact Velocity (m/sec)	Velocity Loss - Δv (m/sec)	Velocity Loss - Δv (m/sec)	Velocity Loss - Δv (m/sec)
Ogive	54	19.27	509.47	49.86	9.05	-
Optimal	50	18.66	507.61	48.07	8.82	-
Cone	47	19.90	491.22	73.09	9.56	26.38
Cone	48	19.73	521.24	73.03	9.57	28.27
Cylinder	44	19.88	445.37	93.45	-	46.53
Cylinder	46	19.90	494.08	99.85	-	49.67

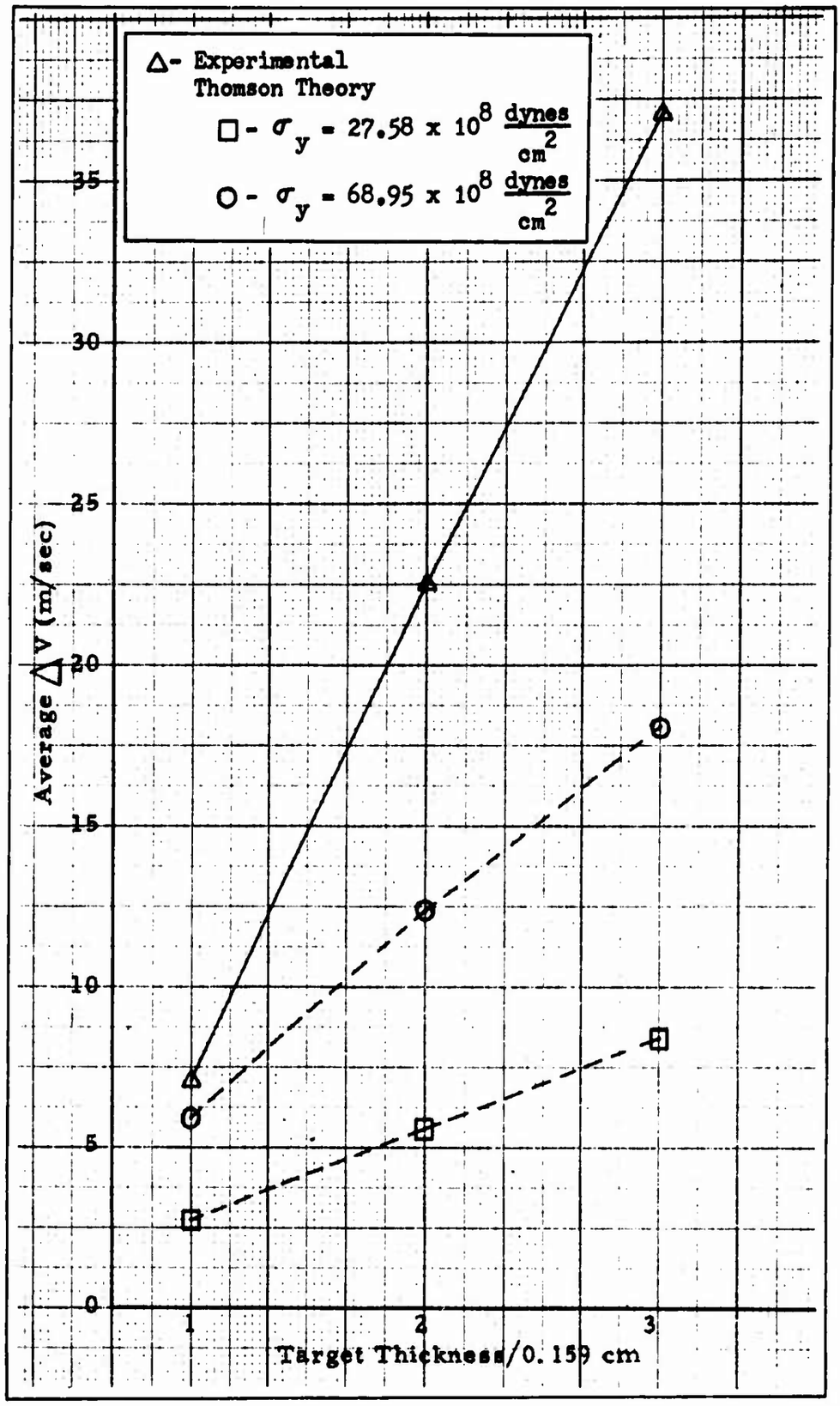

Fig. 10. Theoretical and Experimental Velocity Losses for Ogive Shape (6061-T6 Aluminum Targets)

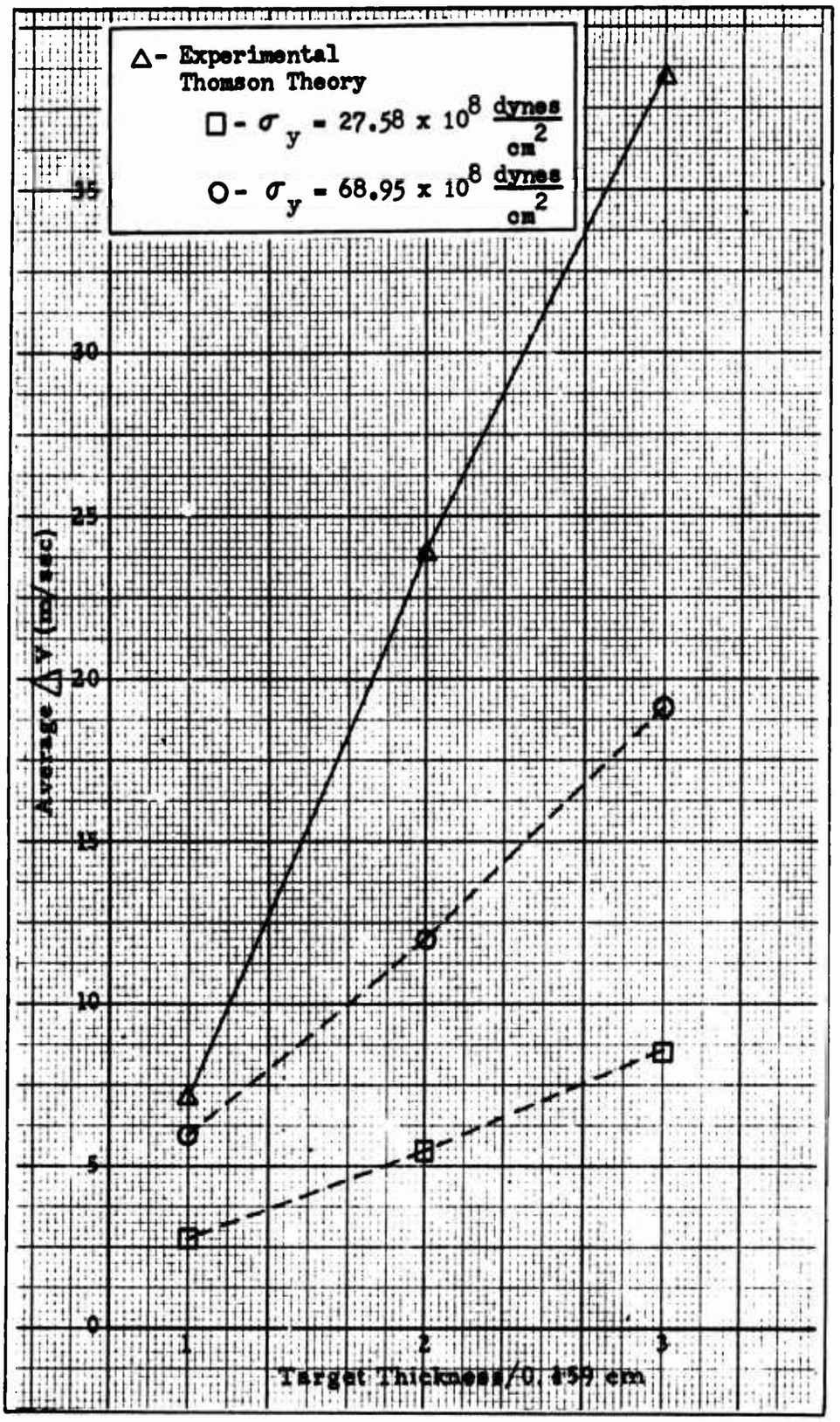

Fig. 11. Theoretical and Experimental Velocity Losses for Optimal Shape (6061-T6 Aluminum Targets)

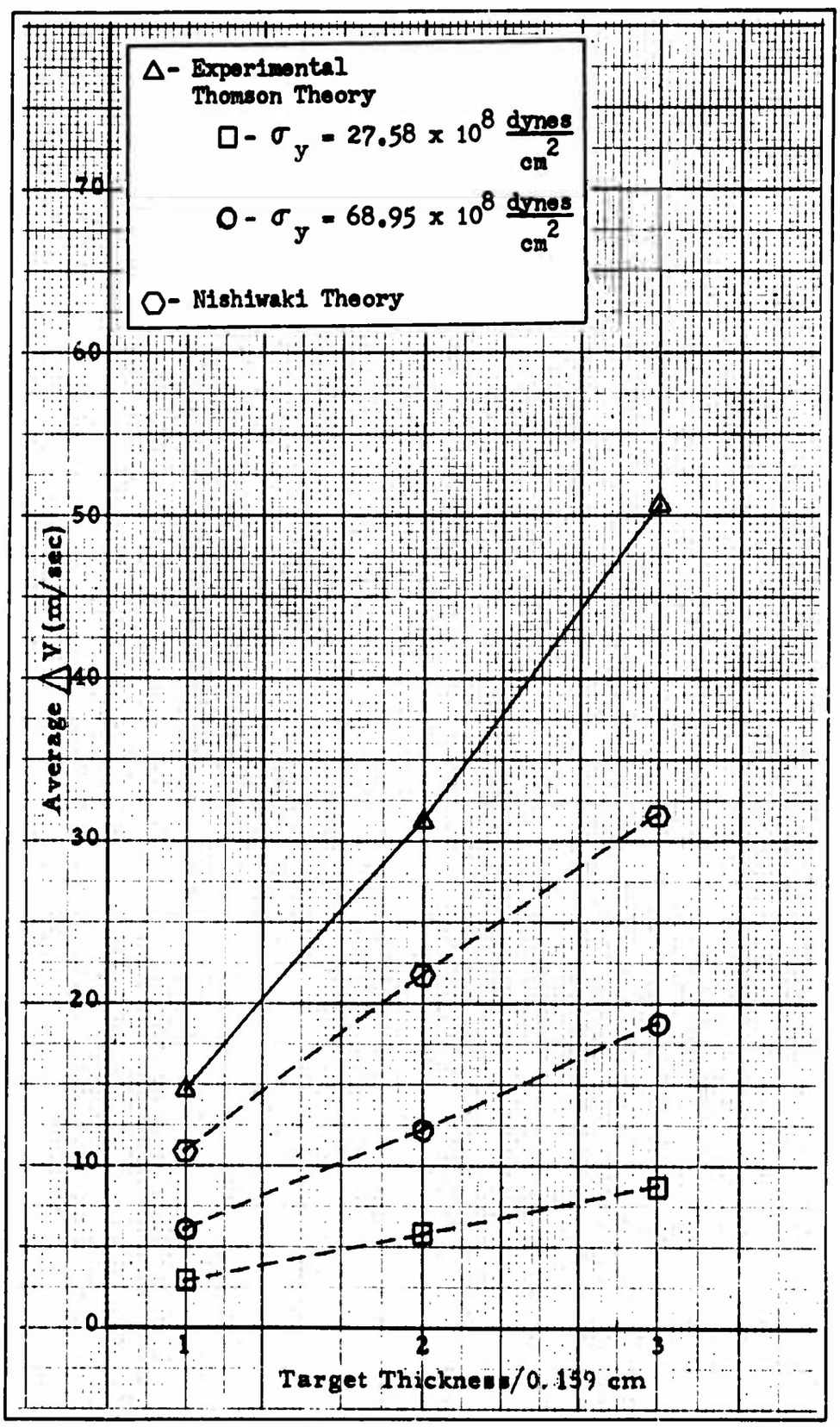

Fig. 12. Theoretical and Experimental Velocity Losses for Cone Shape (6061-T6 Aluminum Targets)

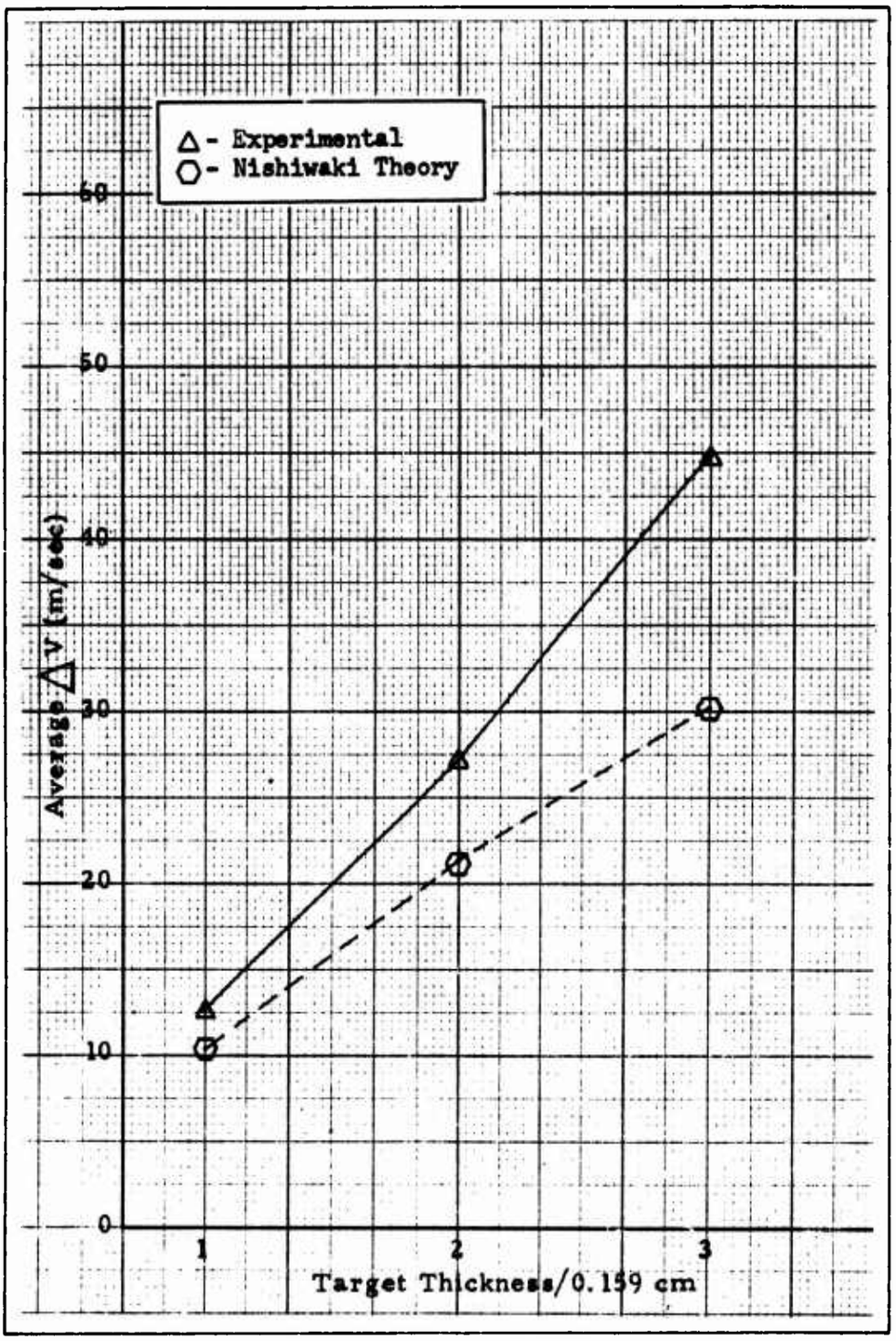

Fig. 13. Theoretical and Experimental Velocity Losses for Cylinder Shape (6061-T6 Aluminum Targets)

agreement. Theory values for a yield stress of 68.95×10^8 dynes/cm^2 are shown in Figs. 10-12 for comparison.

V. Conclusions and Recommendations

Conclusions

Pointed projectiles such as the Ogive and Optimal shapes which cause target petaling during perforation, are more efficient penetrators of thin targets than blunt shapes which plug the target. The combined petaling and plugging target failure observed in the Cone shots, requires more energy than either of the single modes of failure. Small differences in the perforation velocity loss of the Ogive and Optimal projectiles indicate that within some range of pointed ogival shapes, there is little variation in perforation efficiency. While the Russian shape lost more energy than the Ogive and Optimal shapes, the excellent stability of this projectile should make it more effective against bumper type targets.

Calculations made from the two approximate theories predicted velocity losses lower than the experimental values, with the deviations increasing with target thickness and strength. Differences between the Nishiwaki theory and measured values for the Cone and Cylinder projectiles were essentially independent of shape, indicating that better agreement could be achieved with a correction for target material properties. The variation of the Thomson theory from experimental data is more complex, involving both projectile shape and target properties. The energy expended in initial crack formation and in causing target deformations not considered in the theories are the

probable reasons for the deviations between theoretical and experimental data.

Recommendations

The following recommendations are based on the results and experimental methods of this study.

a. Two changes in the ballistic pendulum design and suspension are suggested to increase the measurement accuracy and improve the experimental method. The radio dial cord suspension was subject to changes in length with pendulum weight and temperature and future investigators should consider a less extensible suspension such as steel piano wire. While the large size of the pendulum used in this investigation contributed to the stability of the motion, the fully enclosed box made target access difficult. A design incorporating a frame of similar size, but with a smaller enclosed target area would allow easier access to the target and reduce the problems of projectile stability downrange of the target.

b. Further studies should be made to compare the results of this study with perforation theories. To allow comparison of the Russian data, different curve fitting techniques could be employed to find an analytical expression to describe the nose shape. Additional analysis of the Nishiwaki theory is suggested to obtain better agreement with the experimental data and to extend the theory to allow calculations for ogival shapes.

Bibliography

1. Beers, Yardley. Introduction to the Theory of Error. Cambridge, Mass.: Addison-Wesley Publishing Co., Inc., 1953.

2. Bethe, H. A. "Attempt of a Theory of Armor Penetration" for Frankford Arsenal, 1941.

3. "CORE, .50 cal AP-M2", Industrial Group Ordnance Corp, U.S. Army Ordnance Arsenal, Frankford Arsenal, 1961.

4. Craggs, J. W. "The Normal Penetration of a Thin Elastic-Plastic Plate by a Right Circular Cone." University College, Dundee, October 1952.

5. Den Hartog, J. P. Mechanical Vibrations. New York: McGraw-Hill Book Co., Inc., 1956.

6. Freiberger, W. "A Problem in Dynamic Plasticity: The Enlargement of a Circular Hole in a Flat Sheet." Proc. of Cambridge Phil. Soc., 48:135-148 (1952).

7. Gay, H. P. "Notes of Techniques and Apparatus for Investigating the Effects of Recoil and the Stability of Mounts for Small Arms Weapons." Maryland: Ballistic Research Laboratories Memorandum Rpt. No. 955 (December 1955).

8. Giere, A. C. "Some Energy and Momentum Considerations in the Perforation of Thin Plates." AIAA Journal, 2:8, 1471-1472 (August 1964).

9. Goldsmith, Werner. Impact. London: Edward Arnold (Publishers) Ltd., 1960.

10. Goldsmith, Werner, et al. "Plate Impact and Perforation by Projectiles." Experimental Mechanics, 385-404 (December 1965).

11. Goldsmith, Werner and Ching-Hsie Yew. "Penetration of Conical Indenters Into Plane Metal Surface." 4th Congress of Appl. Mech., 177-188 (1962).

12. Krafft, Joseph M. "Surface Friction in Ballistic Penetration." J. of Appl. Physics, 26:10, 1248-1253 (October 1955).

13. Kucher, V. B. "Optimum Projectile Design for Armor Penetration." Maryland: Ballistic Research Laboratories Rpt. No. 1379 (November 1967).

14. -----. "Penetration With Optimal Work." Maryland: Ballistic Research Laboratories Rpt. No. 1384 (December 1967).

15. Masset, A. Victor. "The Measurement of Forces Resisting Armor Penetration." J. of Appl. Physics, 20:132-140 (February 1949).

16. Metals Handbook, Vol. 1 (Eighth Edition), ASM, 1961.

17. Nishiwaki, Jien. "Resistance to the Penetration of a Bullet Through an Aluminum Plate." J. Phy. Soc. of Japan, 6:374-378 (October 1951).

18. Recht, B. F. and T. W. Ipson. "Ballistic Perforation Dynamics." J. of Appl. Mech., 384-389 (September 1963).

19. Rinehart, John S. and John Pearson. Behavior of Metals Under Impulsive Loads. New York: Dover Publications, Inc., 1960.

20. Spells, K. E. "Velocities of Steel Fragments After Perforation of Steel Plates." Proc. Physical Soc. of London, B, 64:212-218 (1951).

21. Stronge, William J. "Comments on 'Some Energy and Momentum Considerations in the Perforation of Thin Plates'." AIAA Journal, 3:3, 570-571 (March 1965).

22. Swift, H., et al. "An Inexpensive Automatic Digital Film Reader". Paper prepared by the University of Dayton Research Institute, Dayton, Ohio for presentation at the 16th Meeting of the Aeroballistic Range Association, 1969.

23. Taylor, G. I., "The Formation and Enlargement of a Circular Hole in a Thin Plastic Sheet." J. of Mech. and Appl. Math., 1:103-124 (March 1948).

24. Thomson, William T. "An Approximate Theory of Armor Penetration." J. of Appl. Physics, 26:1, 80-82 (January 1955).

25. Wylie, C. R., Jr. Advanced Engineering Mathematics. New York: McGraw Hill Book Co., Inc., 1951.

26. Zaid, Melvin and Paul Burton. "Mechanics of High Speed Projectile Penetration." J. of Franklin Inst., 264:117-126 (1957).

Appendix A

Description of Equipment

The Air Force Materials Laboratory Low Velocity Impact Test Range was used for this study. This facility, located in Building 44, Area B, Wright-Patterson Air Force Base, Ohio, is operated by the University of Dayton Research Institute under Air Force contract. The range equipment, consisting of the gun, sabot catch tank, ballistic pendulum, velocity measurement and flash x-ray systems, is shown in Fig. 14 and is briefly described in this appendix.

Gun

The gun consists of a Frankford Mann universal mount with interchangeable barrels of various calibers. A .50 caliber barrel, rifled for one revolution per 25.4 cm of travel, was used for all data shots while pendulum calibration shots were fired from a standard .308 caliber barrel. The experimental projectiles with sabots were loaded in .50 caliber cartridges and percussion fired by a remotely controlled electric solenoid. A load of 5.31 gm of Dupont IMR 4064 powder was used for all data firings in this series.

Sabot Catch Tank

A steel sabot catch tank was positioned 55.88 cm in front of the gun barrel to trap the copper sabots and contain the muzzle blast. The

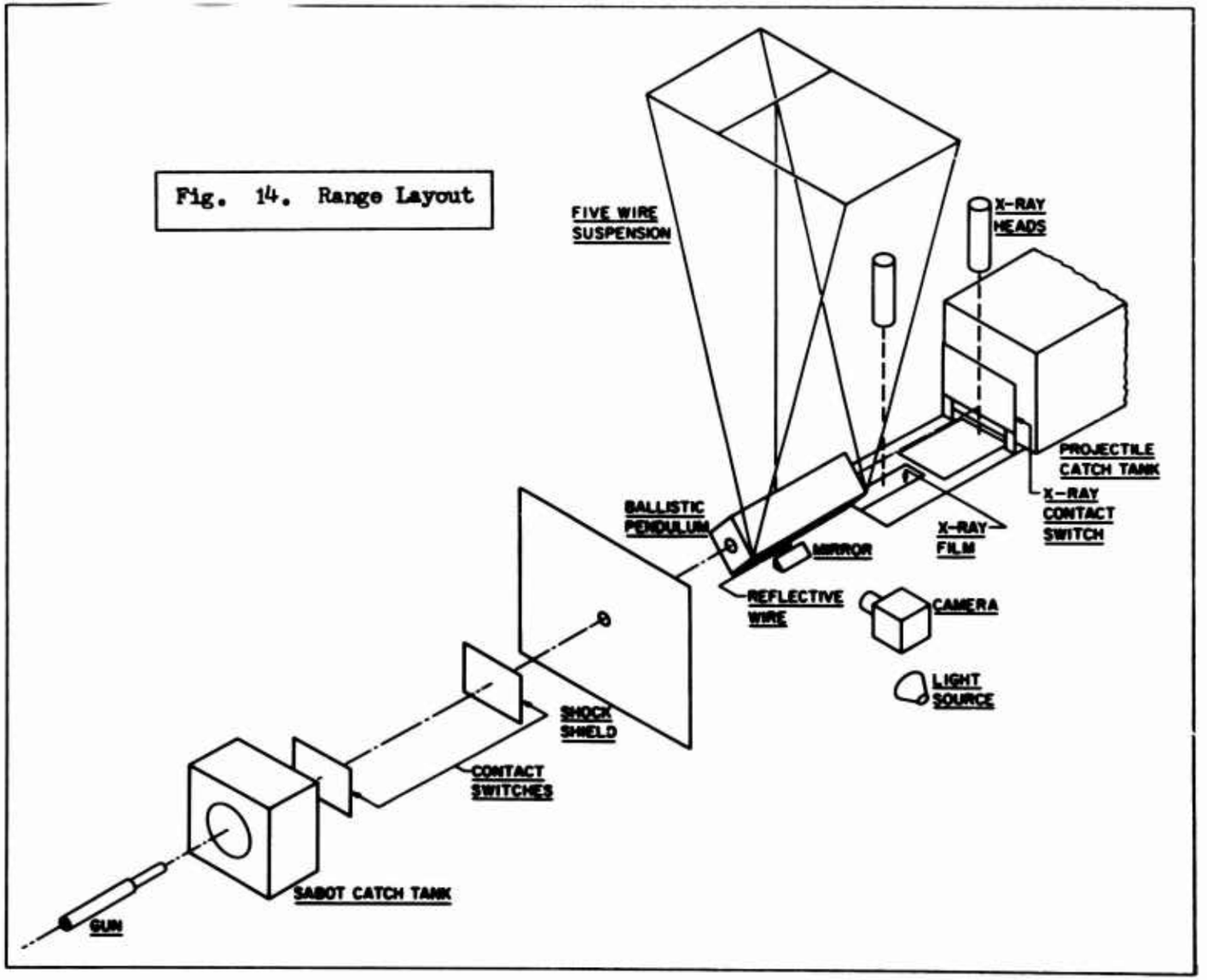

Fig. 14. Range Layout

sabots entered the tank through a 38 cm opening and were stopped in seven layers of 6.4 mm thick plywood. An 8 cm diameter hole through the plywood allowed the unrestricted passage of the projectile through the tank.

Contact Switches

Sandwich-type contact switches constructed of aluminum foil and Mylar were used to trigger the velocity chronographs and x-ray equipment. A layer of 0.03 mm foil with a sheet of 0.013 mm Mylar insulation attached to the front face of the target formed the trigger delay generator switch while the switches for the initial velocity chronograph and second x-ray unit consisted of two layers of foil separated by a sheet of Mylar. A 600 volt potential applied across the switches produced an electrical triggering pulse as the projectile perforated the insulation. Fig. 15 shows a block diagram of the switching circuitry.

Chronographs

The initial projectile velocity was measured over a 1.22 m interval 2.45 m in front of the target. The time between contact switch pulses was recorded to the nearest microsecond with a Beckman Universal EPUT and Timer, Model 7360A. The velocity was calculated within 0.05 m/sec with an average error of ±0.25%. The time between x-ray photographs was recorded on a Beckman/Berkly Universal EPUT and Timer, Model 7370, triggered by the input pulses to the x-ray units.

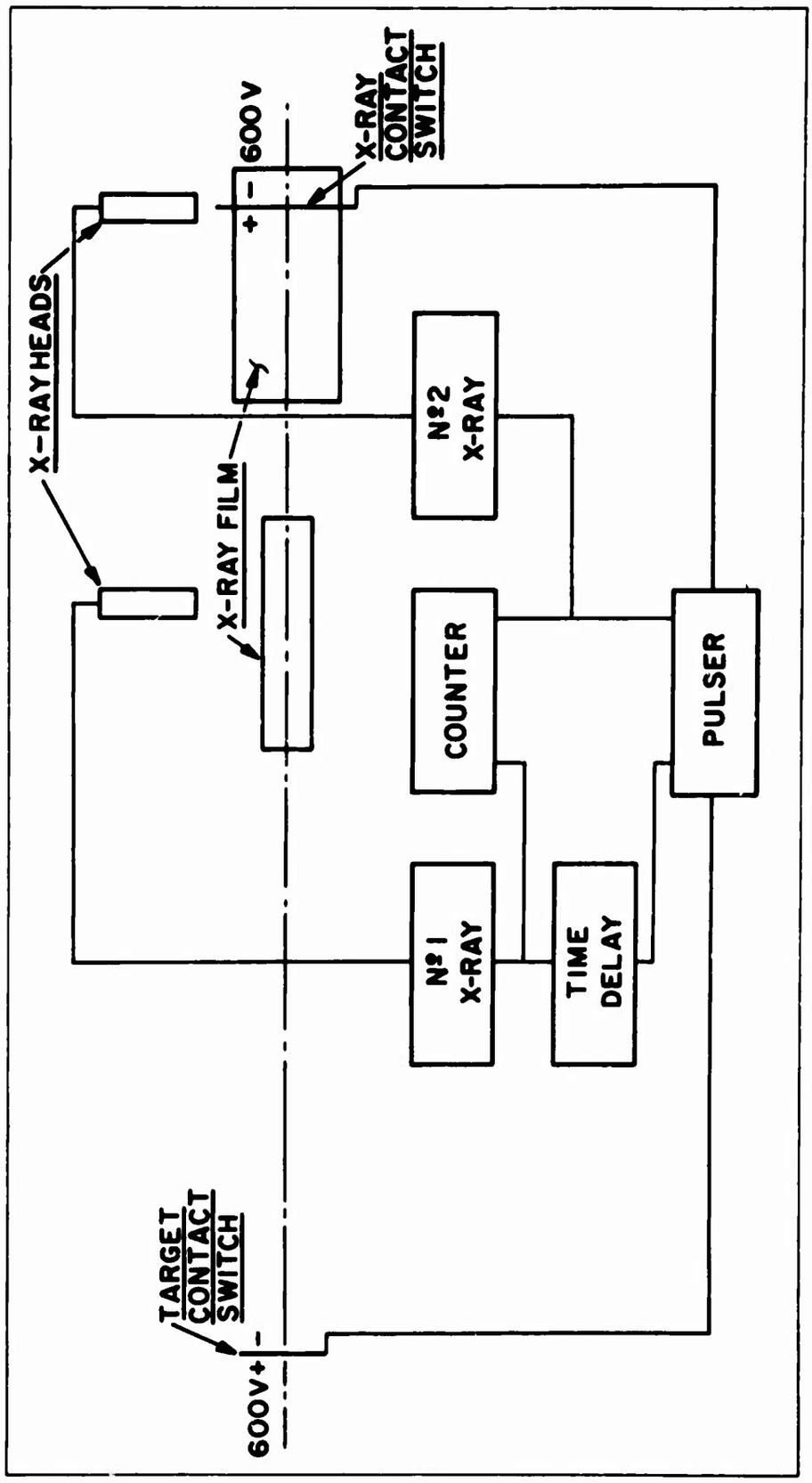

Fig. 15. X-Ray Switching Circuitry

Flash X-ray System

Two 150 kv flash x-ray photographs downrange of the pendulum were used to determine the velocity of target plugs and to check the projectile residual velocity. The equipment consisted of a Field Emission Corporation Model 154, 4 channel control unit; two x-ray heads mounted along and 114 cm above the trajectory; and two film cassettes positioned 26 cm below the centerline (Fig. 14). Triggering of the first x-ray was through a Beckman and Whitley Model 100 Trigger Delay Generator set for a 1450 microsecond delay from the target switch signal. The second x-ray was triggered directly from the rear contact switch.

Ballistic Pendulum

The ballistic pendulum was a rectangular wood box, 76.2 cm in length, with a braced frame made of 2.54 cm x 2.54 cm pine and a 0.32 cm plywood covering on the sides. Construction was symmetric about the axial centerline and the geometric center with a square cross section measuring 25.4 cm on each side and an interior opening of 20.32 cm x 20.32 cm. A plywood bulkhead (Fig. 16) at the center of the frame was designed to accept 14.68 cm x 14.68 cm

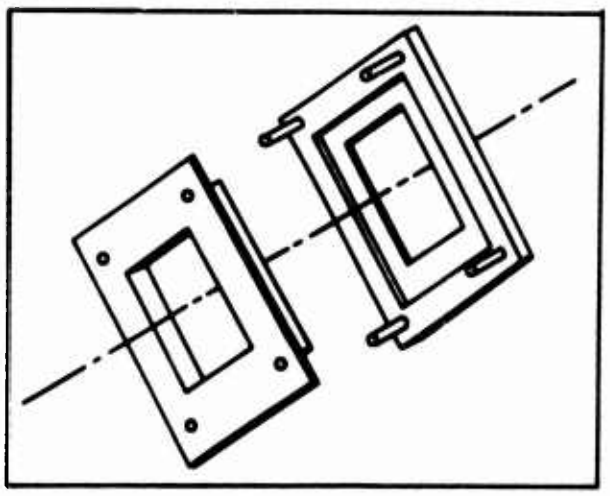

Fig. 16. Target Bulkhead and Face Plate

targets in thicknesses up to 0.635 cm. The targets were locked in position by a removable face plate attached to the bulkhead by 8-32 bolts and wing nuts. A 10.16 cm x 10.16 cm opening through the bulkhead and face plate provided 103.22 cm^2 of target impact area with the target supported equally along each edge over a total area of 112.28 cm^2. Metal contacts in the bulkhead and face plate connected the target switch to the trigger delay generator.

Pendulum Fittings. The interior length of the pendulum on each side of the target was lined to contain target debris and to protect the basic frame. The removable liner was an open rectangular box constructed of 0.32 cm thick poster board covered with two layers of 0.16 cm thick ballistic felt. Square end plates, measuring 25.4 cm x 25.4 cm, made of 0.32 cm thick tempered masonite were attached to the pendulum with 8-32 bolts and wing nuts. A 0.63 cm thick layer of ballistic felt was glued to the inside face of the end plates to absorb target debris and a 6.35 cm diameter hole allowed projectile entry and exit. To change the pendulum weight, steel plates were attached to the sides with 10-24 bolts and wing nuts. The average mass of the basic pendulum was 4520 gm.

Pendulum Suspension. The pendulum was suspended with radio dial cord in the five wire configuration described by Gay (Ref 7:6-10) and shown in Fig. 17. Aluminum beams attached to a 3.7 m high scaffolding formed a level ceiling plane for the 2.44 m suspension system while three 0.32 cm thick brass pendulum supports formed a

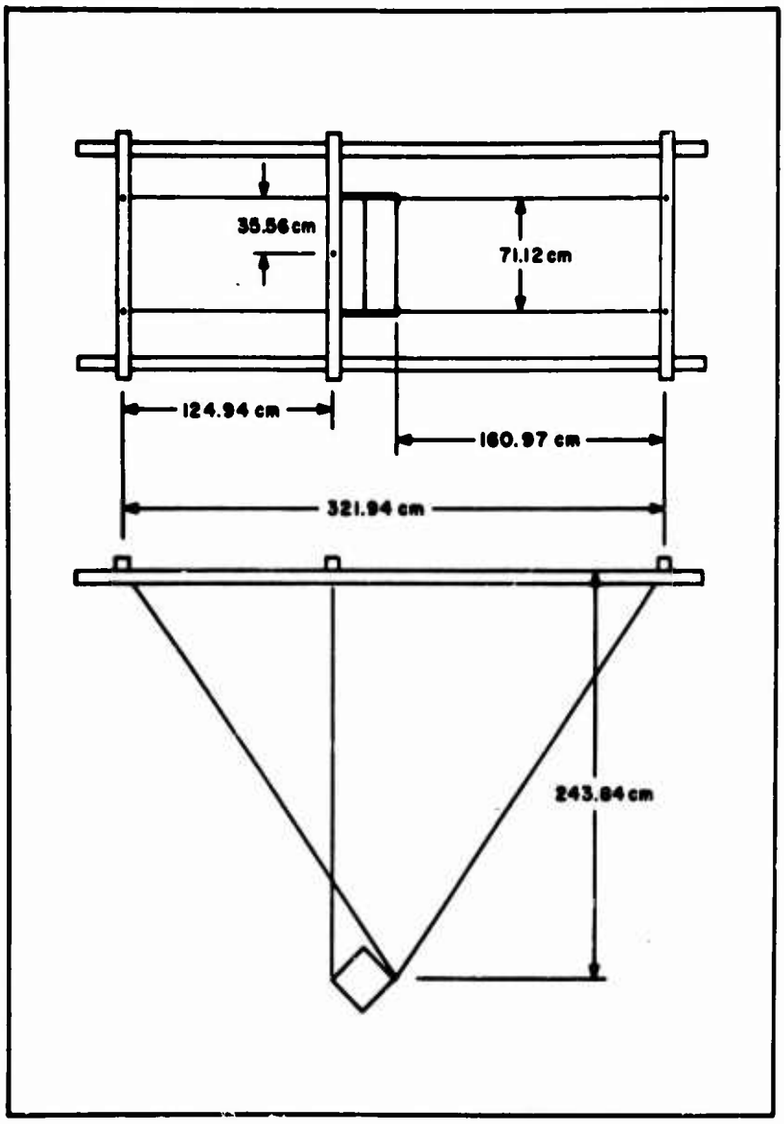

Fig. 17. Pendulum Suspension

pendulum support plane through the center of the pendulum. To eliminate hinge moments and keep the pivot axes in the support planes, the dial cord was passed through 1.6 mm holes in the supports and fastened on the opposite sides.

Pendulum Instrumentation. A piece of tinned wire attached to the bottom of the pendulum served as a light reflector for monitoring the pendulum motion. A mirror and reference scale were mounted on a tripod which was adjusted to keep the scale at the level of the reflector. A bottom view of the reflector and scale was reflected in the silvered mirror and photographed with an open shutter Burke and James View Camera positioned 90 degrees to the pendulum path. Polaroid 255A positive-negative film was used with an f.22 lens setting and a standard photoflood light source. This system is shown in Fig. 18.

Automatic Digital Film Reader

An automatic digital film reader was used to read the photograph negatives of the pendulum motion. With this sytem, shown in Fig. 19 and described in detail in Ref. 22, the deflections were measured to an accuracy of 0.08 mm. This unit, coupled to an IBM Model 26 cardpunch, was also used to obtain coordinates of projectile nose curves.

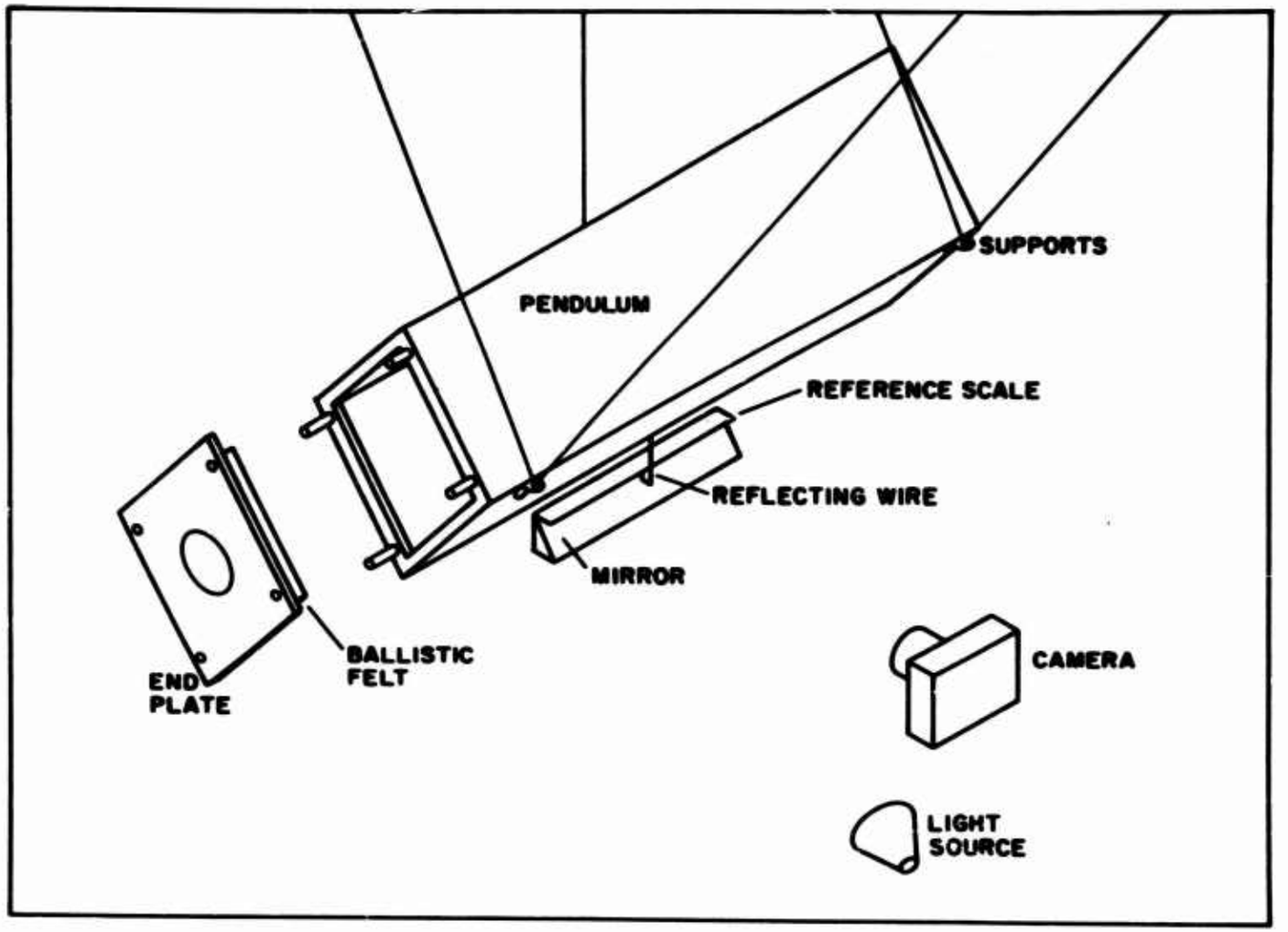

Fig. 18. Pendulum Instrumentation

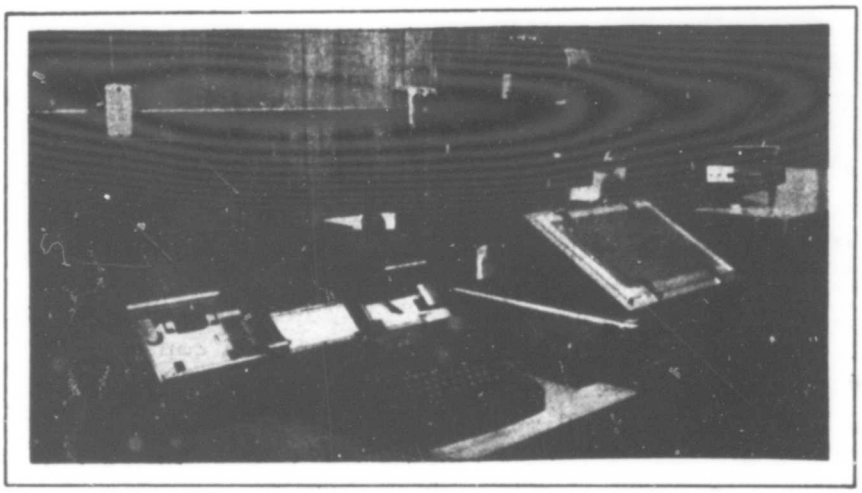

Fig. 19. Automatic Digital Film Reader

Appendix B

Projectile Design

Two ballistics problems encountered in this study were projectile design and the development of a method for launching unjacketed projectiles at a velocity of 518 m/sec, with sufficient stability to achieve normal target impact. The location of the target at the center of the ballistic pendulum placed an additional requirement for projectile stability after target perforation in order for the projectiles to clear the rear of the pendulum. To solve these problems, spin stabilization tests were conducted with discarding sabot projectiles fired from a rifled .50 caliber barrel.

In early trials, both standard .50 caliber cores and conical nosed projectiles made of 1.11 cm diameter tempered steel drill rod were fired with plastic sabots, leather patch sabots and sabots made of two halves of split copper tubing. Due to inadequate friction between the sabot and projectile, these launch methods failed to achieve appreciable projectile spin. A partially successful technique was the use of the split copper tubing sabot, notched to grip a square which was machined on the rear of the projectile (see Fig. 20).

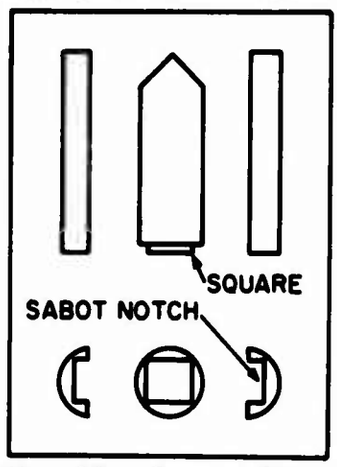

Fig. 20. Square Base Copper Sabot

To maintain launch integrity, the sabot was soldered to the base of the projectile. Good projectile spin was achieved with this method, but aerodynamic instability occurred on some shots which was attributed to uneven sabot separation. Although these tests were unsuccessful, the results were useful in the design of the final launch configuration.

Projectile Sabots

In the data gathering phase of this experiment, projectiles were launched with copper sabots crimped into two v-notches in the side of the projectile. Half-hard copper tubing with an outside diameter of 1.27 cm and a 0.89 mm wall thickness was cut in 3.49 cm lengths and split lengthwise to form the two sabot halves. The 90 degree v-notches were machined on opposite sides of the projectile, 0.95 cm from the base and the sabots were crimped into the notches with a special crimping die (Fig. 21). A 0.8 mm wide, 0.127 mm deep groove was cut in the outer circumference of the sabot. This groove, located 6.4 mm from the base, formed a ring into which the cartridge was crimped during loading. The launch configuration is shown in Fig. 22.

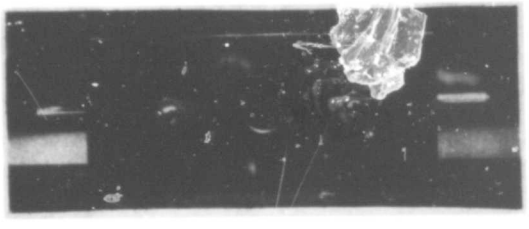

Fig. 21. Sabot Crimping Die

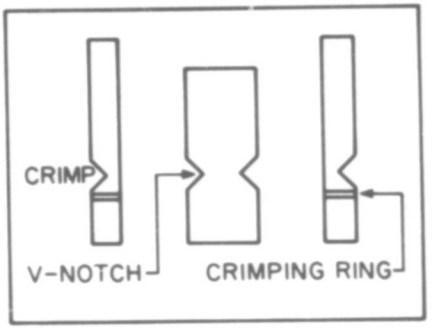

Fig. 22. Experimental Sabot

Experimental Projectiles

The experimental projectiles were machined from 1.11 cm diameter tempered steel drill rod with the overall length and mass distribution adjusted to achieve suitable stability after target perforation. Fig. 23 shows the projectile dimensions and Fig. 23 is a photograph of the actual projectiles and sabots.

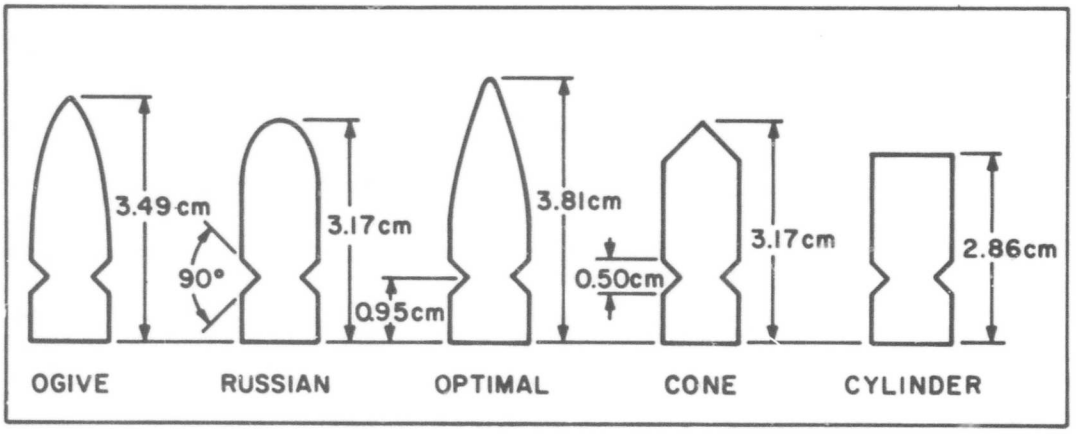

Fig. 23. Projectile Dimensions

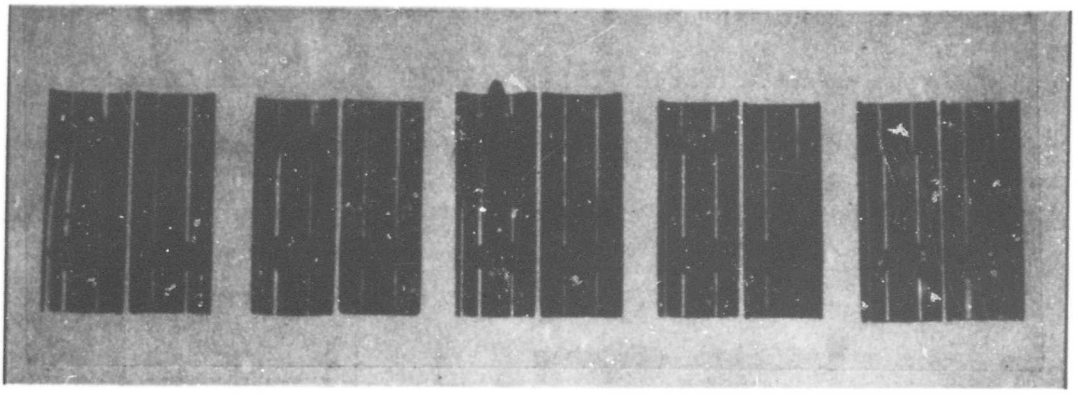

Fig. 24. Experimental Projectiles and Sabots

Ogive Shape. This projectile, referred to as the "Ogive", was 3.49 ± 0.01 cm long with an average mass of 19.31 gm. The nose

shape was patterned from a machine drawing of the core of a U. S. 50 caliber armor piercing bullet.

Russian Shape. The "Russian" shape was patterned from an armor piercing core from a 14. 5 mm Russian bullet (Ref 3). The length was 3. 17 ± 0. 01 cm with the base center drilled to a depth of 0. 32 cm, giving an average mass of 19. 66 gm.

Optimal Shape. The "Optimal" projectile was shaped from Kucher's equation (Ref 13:11) of an optimal penetrator for thin armor plate. The total length was 3. 49 ± 0. 01 cm with an average mass of 19. 38 gm for the projectiles used against the 1. 59 mm and 3. 17 mm aluminum targets. For shots against the 4. 76 mm aluminum and 1. 59 mm steel targets, the projectile bases were center drilled to a depth of 1. 11 cm and the forward 0. 8 cm of the hole filled with lead to shift the mass center forward. The average mass of these projectiles was 18. 59 gm.

Cone. This projectile was 3. 17 ± 0. 01 cm in length with a 45 degree conical nose. The base was center drilled to a depth of 0. 32 cm, giving an average projectile mass of 19. 7 gm.

Cylinder. The cylindrical shape was 2. 86 ± 0. 01 cm long with an average mass of 19. 88 gm.

Appendix C

Ballistic Pendulum Alignment and Calibration

Pendulum Alignment

Final adjustments in pendulum alignment were made using a Watkins Johnson Model 291 Laser. The laser was bore sighted through the gun barrel to provide a visible range centerline and the longitudinal axis of the pendulum was then aligned with the trajectory. The laser beam, reflected from a mirror mounted in the target position, was used to align the target and to eliminate side and rocking motion of the pendulum. Plywood shims were glued to the support face of the target holder to achieve a target orientation normal to the trajectory, indicated by the superposition of the reflected and incident laser beams. To obtain level, linear motion, the pendulum was placed in motion and small adjustments made in the suspension until the reflected laser beam remained stationary on the incident beam. To eliminate rolling motion, a mirror was attached to the side of the pendulum and the laser aligned to superpose the incident and reflected beams. The pendulum was again set in motion and small suspension adjustments made to keep the laser beams superimposed.

Pendulum Period

The period of the lateral pendulum motion was determined from five measurements of the time to complete ten cycles. Measurement

over a larger number of cycles was impossible as the motion was essentially damped out after ten periods. A chronograph was manually triggered to record the times to the nearest 1/10 of a millisecond with the results shown in Table IX.

Table IX

Lateral Period Calibration

Test No.	Number of Periods	Time (sec)	Period (sec)
1	10	4.3880	0.4388
2	10	4.4556	0.4456
3	10	4.9246	0.4925
4	10	4.5026	0.4503
5	10	4.1617	0.4162
	Average Period:	0.448 sec	

The longitudinal period was measured by timing thirty pendulum cycles before and after each data shot. A chronograph, triggered by a pendulum switch, recorded the times to the nearest 1/10 millisecond. The switch consisted of two fine wires attached to a board which was raised into position to allow the wires to contact the brass pendulum support (Fig. 25). At contact, a 600 volt potential applied across the wires created an electrical arc which triggered the chronograph. To minimize the drag on the pendulum, the contact wires were made of watch spring steel. The switch was mounted to make contact with the support at the center of the pendulum swing with a maximum variation

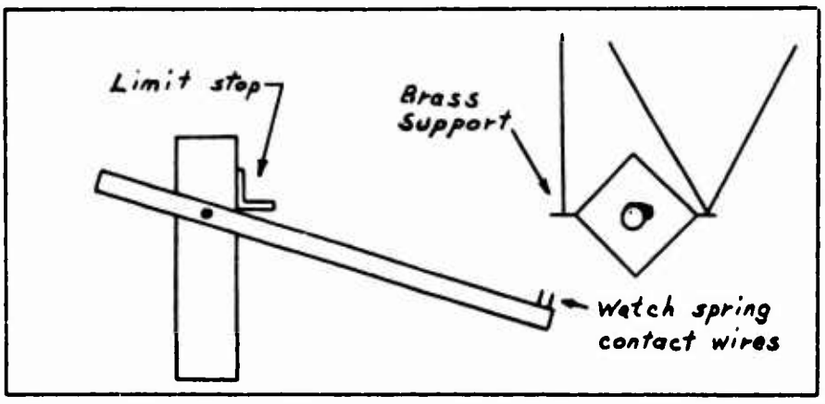

Fig. 25. Pendulum Timing Switch

between the switch positions at the start and end of a timing cycle of 3 mm, caused by slight deflections of the contact wires.

Pendulum Damping

Pendulum damping forces were evaluated by calculating the decrease in amplitude per cycle of the free swinging pendulum. Successive values of pendulum amplitude were measured from timed photographs of the 1st, 10th, 20th, 30th and 40th swings of the pendulum. Six damping tests were made to cover the range of amplitudes obtained on data shots. Treating the forces as a damped free vibration, the amplitudes were related by:

$$x_n = x_m e^{k(n-m)} \tag{27}$$

where x_n is the amplitude of the nth swing, x_m is the amplitude of the mth swing, and k is the damping coefficient (Ref 5:37). Values of k were calculated for each amplitude measured and for each change in pendulum configuration. To obtain the undamped pendulum amplitude,

the damping correction for one quarter of a cycle was applied to the measured amplitude through the relation:

$$x_o = x_1 e^{-k/4} \tag{28}$$

Pendulum Calibration Shots

The ballistic pendulum was calibrated with 1.04 gm steel spheres fired into the pendulum from a .308 caliber barrel. A wood block with an 8.89 cm x 8.89 cm target area and a length of 10.16 cm was used as the target for stopping the spheres. The sphere velocity was calculated from the measured time to travel 32.61 cm between two contact switches in the pendulum. The switches were mounted on the pendulum front end plate and on the face of the target block and the time was recorded to the nearest microsecond with a chronograph.

The horizontal pendulum displacement, measured from photographs of the motion, was used to calculate the pendulum momentum from the relation:

$$m_p v_p = \frac{2\pi c m_p}{T} \tag{29}$$

where m_p is the pendulum mass, v_p is the pendulum velocity, T is the pendulum period and c is the chord of the pendulum arc (Ref 7:7-8). In computing the momentum, the chord, c, was replaced by the measured value, d (Fig. 26). For the suspension length, L, of 243.84 cm and a maximum displacement, d, of 3.2 cm, the maximum

error resulting from this substitution was 0.0003 cm or 0.009%. The results of the calibration are given in Table X.

Aerodynamic Drag

To determine a correction factor for the momentum imparted to the pendulum through aerodynamic drag, each projectile shape was fired through the pendulum with a sheet of 0.013 mm Mylar mounted as a target. The Mylar served as an effective target for the drag forces while producing negligible resistance to projectile perforation. An assumed drag force proportional to the square of the velocity was used in the equation of motion to give:

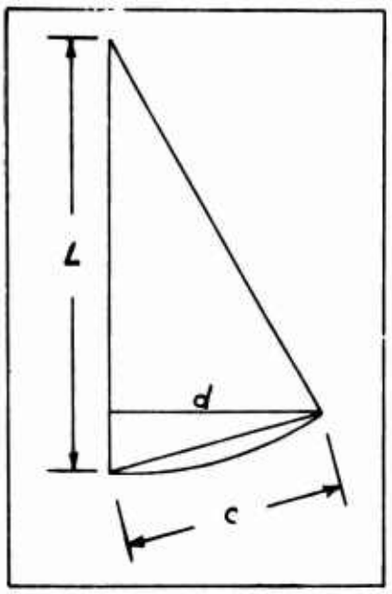

Fig. 26. Pendulum Displacement

$$D = k_D v^2 = m\frac{dv}{dt} \tag{30}$$

where m is the projectile mass; v is the projectile velocity; and k_D is a drag coefficient. Changing variables, the equation becomes:

$$k_D v^2 = mv\frac{dv}{dx} \quad \text{or} \quad \frac{k_D}{m}dx = \frac{dv}{v} \tag{31}$$

and upon integration:

$$\frac{k_D}{m}(x_2-x_1) = \ln\left(\frac{v_2}{v_1}\right) \quad \text{or} \quad v_2 = v_1 e^{\frac{k_D}{m}(x_2-x_1)} \tag{32}$$

Values of k_D were calculated for each projectile from the drag test

Table X

Pendulum Calibration

Shot No.	Mass (gm)	Impact Velocity (m/sec)	Momentum (gm-cm/sec)	Mass (gm)	Chord (cm)	Period (sec)	Momentum (gm-cm/sec)	Percent Difference
X3	1.04	582.78	60,609.12	10,210.14	2.951	3.1390	60,310.16	0.49
X4	1.04	598.20	62,212.80	10,212.22	3.071	3.1386	62,783.41	0.92
X6	1.04	591.89	61,556.56	10,209.50	2.987	3.1371	61,079.04	0.78
11	1.04	337.99	35,150.96	5,227.04	3.177	3.1434	35,440.10	0.82

measurements, assuming a constant momentum loss over the pendulum length. These values, listed in Table XI, were used to correct the pendulum and velocity measurements of data shots.

Table XI

Aerodynamic Drag Calibration

Shot No.	Shape	Pendulum Chord (cm)	Pendulum Mass (gm)	Pendulum Momentum gm-cm/sec)	Projectile Mass gm	k_D gm/cm
60	Optimal	0.055	5163.3	567.62	18.47	-3.502×10^{-4}
61	Russian	0.085	5163.3	877.24	19.84	-5.949×10^{-4}
62	Cone	0.145	5163.3	1496.47	19.64	-9.640×10^{-4}
64	Ogive	0.076	5163.3	784.35	19.29	-4.759×10^{-4}
66	Cylinder	0.166	5163.3	1711.65	19.91	-14.945×10^{-4}

Appendix D

Data and Data Reduction

In this investigation, data was obtained from three basic measurement techniques; a chronograph for initial velocity; the ballistic pendulum for projectile velocity losses; and timed x-ray photographs for residual and plug velocities. The basic data is given in Tables XII through XVII.

Initial Velocity Data

The initial projectile velocity was determined from measurements of the time to travel a measured distance between the initial velocity contact switches. A chronograph recorded the time to the nearest microsecond and the velocity was calculated to the nearest 0.05 m/sec with a maximum error of ±0.25%. Aerodynamic drag calculations described in Appendix C, were applied to this velocity to determine the target impact velocity.

Ballistic Pendulum Data

The pendulum data was reduced in the same manner as for the calibration shots described in Appendix C. Horizontal pendulum displacements measured to the nearest 0.08 mm with the Automatic Film Reader (Appendix A), were taken as the chord of the pendulum arc. To correct for parallax, the measured chord was reduced by the

Table XII

Data for 0.159 cm 6061-T6 Aluminum Targets

Projectile				Pendulum				
Shape	Shot No.	Mass (gm)	Initial Velocity (m/sec)	Period (sec)	Mass (gm)	Measured Chord (cm)	Corrected Chord (cm)	Δv_p (m/sec)
Ogive	2	19.34	538.76	3.1398	6046	1.323	1.153	7.22
Ogive	3	19.25	532.85	3.1459	6045	1.280	1.112	6.98
Optimal	4	19.35	519.93	3.1456	6031	1.280	1.156	7.19
Optimal	5	19.37	521.02	3.1459	6044	1.275	1.151	7.16
Russian	7	19.73	511.64	3.1480	6174	2.185	1.979	12.34
Russian	57	19.75	502.74	3.1429	6376	1.923	1.737	12.53
Cone	9	19.70	513.13	3.1450	6177	1.215	0.899	5.64
Cone	10	19.71	521.48	3.1460	6177	1.141	0.820	5.17
Cylinder	58	19.89	484.57	3.1434	6376	1.072	0.632	4.05
Cylinder	59	19.88	518.16	3.1431	6376	0.963	0.500	3.20

Table XIII

Data for 0.317 cm 6061-T6 Aluminum Targets

Projectile				Pendulum				
Shape	Shot No.	Mass	Initial Velocity (m/sec)	Period (sec)	Mass (gm)	Measured Chord (cm)	Corrected Chord (cm)	ΔV_p (m/sec)
Ogive	13	19.39	-*	3.1388	10,823	2.162	2.065	23.07
Ogive	14	19.32	-*	3.1394	10,823	2.254	2.154	24.14
Ogive	56	19.28	558.73	3.1447	10,977	1.918	1.808	20.57
Optimal	12	19.31	520.81	3.1610	10,811	2.129	2.047	22.77
Optimal	15	19.59	-*	3.1397	10,801	2.323	2.240	24.72
Optimal	16	19.24	530.53	3.1397	10,803	2.279	2.195	24.66
Optimal	19	19.41	522.15	3.1396	10,797	2.156	2.075	23.10
Optimal	41	18.59	-*	3.1448	10,985	2.136	2.062	24.35
Russian	23	19.82	531.91	3.1389	10,790	2.388	2.258	24.60
Russian	25	19.80	501.52	3.1395	10,795	2.550	2.423	26.43
Cone	22	19.78	537.09	3.1397	10,802	1.643	1.450	15.85
Cone	24	19.82	511.85	3.1385	10,790	1.399	1.217	13.26
Cylinder	26	19.87	489.63	3.1393	10,796	1.018	0.757	8.23
Cylinder	27	19.89	489.45	3.1393	10,796	1.270	1.008	10.94

* Chronograph failed - impact velocity calculated from x-ray data.

Table XIV

Data for 0.476 cm 6061-T6 Aluminum Targets

Projectile				Pendulum				
Shape	Shot No.	Mass (gm)	Initial Velocity (m/sec)	Period (sec)	Mass (gm)	Measured Chord (cm)	Corrected Chord (cm)	ΔV_p (m/sec)
Ogive	28	19.32	532.85	3.1395	11,072	3.256	3.144	36.06
Ogive	29	19.28	523.25	3.1399	11,070	3.447	3.335	38.31
Optimal	39	18.29	491.22	3.1421	11,075	3.487	3.401	41.18
Optimal	40	18.82	528.46	3.1419	11,076	3.132	3.045	35.84
Russian	31	19.79	507.58	3.1395	11,068	3.823	3.688	41.27
Russian	42	19.24	499.87	3.1446	11,083	3.828	3.693	42.49
Cone	32	19.79	518.59	3.1397	11,070	2.923	2.733	30.60
Cone	33	19.69	526.42	3.1393	11,071	2.405	2.215	24.93
Cone	43	19.92	477.56	3.1437	11,082	2.852	2.669	29.69
Cone	55	19.76	520.78	3.1458	11,080	2.964	2.771	31.03
Cylinder	34	19.87	506.52	3.1401	11,070	2.108	1.836	20.48
Cylinder	36	19.88	498.04	3.1412	11,066	2.090	1.821	20.27

Table XV

Data for 0.317 cm 1030 Steel Targets

Projectile				Pendulum				
Shape	Shot No.	Mass (gm)	Initial Velocity (m/sec)	Period (sec)	Mass (gm)	Measured Chord (cm)	Corrected Chord (cm)	Δv_p (m/sec)
Ogive	54	19.27	512.49	3.1456	11,220	4.404	4.287	49.86
Optimal	50	18.66	509.90	3.1458	11,259	4.079	3.988	48.07
Russian	49	19.20	-*	3.1455	11,295	4.122	3.993	57.70
Russian	53	19.81	493.81	3.1459	11,139	4.275	4.143	61.11
Cone	47	19.90	-*	3.1462	11,255	2.609	2.436	28.68
Cone	48	19.73	527.33	3.1457	11,251	2.502	2.311	26.33
Cylinder	44	19.88	453.39	3.1423	11,294	3.889	3.630	41.24
Cylinder	46	19.90	502.98	3.1459	11,298	4.074	3.792	43.01

* Chronograph failed - impact velocity calculated from x-ray data.

Table XVI

X-ray Plug Data

Target	Shape	Shot No.	Plug Mass (gm)	X-ray Velocity (m/sec)	Projectile Velocity Loss (m/sec)
0.159 cm 6061-T6 Aluminum	Cone	9	0.372	479.27	9.05
	Cone	10	0.385	496.43	9.64
	Cylinder	58	0.411	468.69	9.70
	Cylinder	59	0.411	400.14	8.26
0.317 cm 6061-T6 Aluminum	Cone	22	0.661	-*	16.64*
	Cone	24	0.701	448.91	16.79
	Cylinder	26	0.806	452.93	18.38
	Cylinder	27	0.716	471.46	16.98

* Chronograph failed - plug velocity assumed equal to residual projectile velocity.

Table XVII

X-ray Plug Data

Target	Shape	Shot No.	Plug Mass (gm)	X-ray Velocity (m/sec)	Projectile Velocity Loss (m/sec)
0.476 cm 6061-T6 Aluminum	Cone	32	0.978	437.14	21.61
	Cone	33	0.969	471.86	23.23
	Cone	43	0.992	414.59	20.63
	Cone	55	0.873	463.30	24.57
	Cylinder	34	1.048	461.65	24.36
	Cylinder	36	1.071	456.07	24.57
0.317 cm 1030 Steel	Cone	47	2.081	407.43	44.41
	Cone	48	2.085	441.90	46.70
	Cylinder	44	2.782	373.11	52.21
	Cylinder	46	2.685	421.39	56.84

correction shown in Fig. 27. Aerodynamic drag and pendulum damping correction were applied to obtain the corrected chord which represented the pendulum displacement due to the projectile momentum lost by the projectile in target perforation.

The longitudinal period of the pendulum swing was measured before and after each data shot, with an average of the two values taken as the period. The mass of the basic pendulum box was measured daily with a comparator balance while the mass of the target, liners and end plates were determined by weighing the components before and after each shot. Four steel plates with a total mass of 4.532 kg were added to the pendulum to control the swing on shots against the thicker targets. The total pendulum mass used in the calculations was the sum of the basic frame and all fittings.

X-ray Measurements

The basic purpose of the flash x-ray measurements was to determine plug velocities for the Cone and Cylinder shots. On six tests, the initial velocity chronograph failed and the projectile velocity was determined from the x-ray photographs. These values were corrected for aerodynamic drag to determine the target impact velocity.

Relative positions between the two x-rays were measured with a scale prepared from x-ray photographs of a reference positioned along the trajectory. Wire cross hairs on each film holder provided an orientation reference for aligning the data photographs. The time

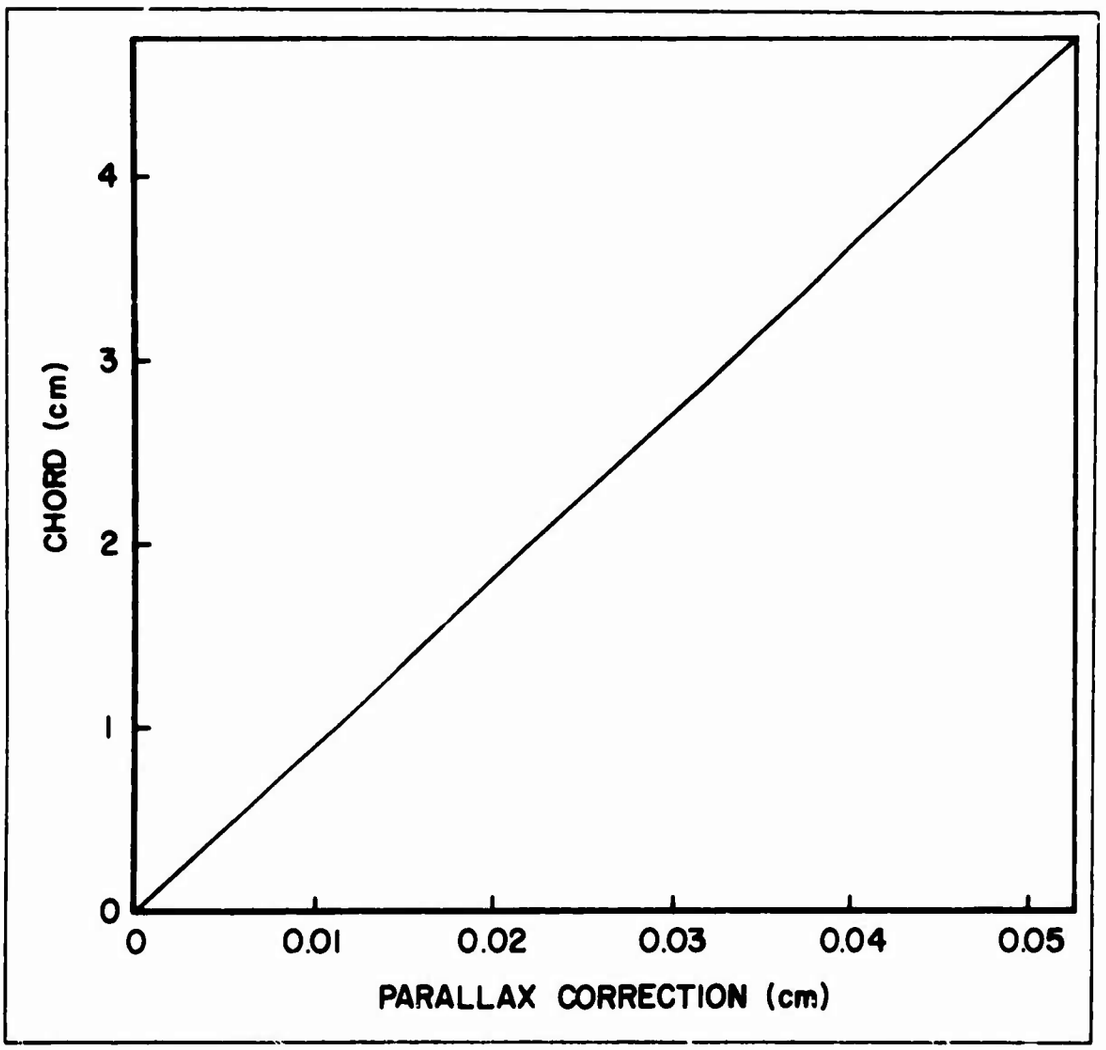

Fig. 27. Parallax Correction Chart

between x-rays, within ± 4 microseconds, was recorded on a chronograph and the measured time and distance used to calculate plug velocity. This velocity and the mass of the recovered plug were used to determine the projectile momentum imparted to the plug.

On shot no. 22 the x-ray chronograph failed and the plug velocity was calculated, assuming a plug velocity equal to the residual projectile velocity. The validity of this assumption for the Cone plugs is supported by photographs from the other data shots. The projectile velocity losses given in Tables XVI and XVII are the losses due to plug momentum and the total projectile loss is the sum of this value and the pendulum loss, ΔV_p.

Unclassified
Security Classification

DOCUMENT CONTROL DATA - R & D

(Security classification of title, body of abstract and indexing annotation must be entered when the overall report is classified)

1. ORIGINATING ACTIVITY *(Corporate author)*
Air Force Materials Laboratory
Wright-Patterson AFB, Ohio 45433

2a. REPORT SECURITY CLASSIFICATION
Unclassified

2b. GROUP

3. REPORT TITLE
THE EFFECT OF PROJECTILE SHAPE ON THE BALLISTIC PERFORATION OF THIN METAL PLATES

4. DESCRIPTIVE NOTES *(Type of report and inclusive dates)*
Technical Report

5. AUTHOR(S) *(First name, middle initial, last name)*
Major Thomas E. Fields

6. REPORT DATE	7a. TOTAL NO. OF PAGES	7b. NO. OF REFS
July 1969	73	26

8a. CONTRACT OR GRANT NO.

b. PROJECT NO.
7360

c.
Task No. 736006

d.

9a. ORIGINATOR'S REPORT NUMBER(S)
AFML-TR-69-202

9b. OTHER REPORT NO(S) *(Any other numbers that may be assigned this report)*

10. DISTRIBUTION STATEMENT
This document has been approved for public release and sale; its distribution is unlimited.

11. SUPPLEMENTARY NOTES

12. SPONSORING MILITARY ACTIVITY
Air Force Materials Laboratory
Air Force Systems Command
Wright-Patterson AFB, Ohio 45433

13. ABSTRACT

The effect of projectile shape on thin target perforation was investigated for five projectile shapes impacting aluminum and steel targets at 506 m/sec. A discarding sabot technique was developed for launching the unjacketed steel projectiles and accurate perforation velocity losses were measured using a ballistic pendulum with the targets mounted in the center of the pendulum. The five projectile shapes included two pointed ogives, a shape similar to a Russian 14.5 mm AP core, a cylinder and a cone. The two ogive shapes were the most efficient penetrators while the velocity loss of the Russian projectile averaged 15% higher. The cone, which caused a combined petaling and plugging target failure, was the least effective shape. Calculations with two approximate perforation theories predicted smaller velocity losses than were found experimentally.

DD FORM 1 NOV 68 1473

Unclassified
Security Classification

14. KEY WORDS	LINK A		LINK B		LINK C	
	ROLE	WT	ROLE	WT	ROLE	WT
Perforation						
Ballistic Impact						
Ballistic Pendulum						
Projectile Shape						